Pergamon

Geochimica et Cosmochimica Acta, Vol. 63, No. 13/14, pp. 2123–2143, 1999

0016-7037/99 $20.00 + .00

PII S0016-7037(99)00189-1

Petrogenesis of silicate inclusions in the Weekeroo Station IIE iron meteorite: Differentiation, remelting, and dynamic mixing

ALEX RUZICKA,*[,1] GRANT W. FOWLER,[2,†] GREGORY A. SNYDER,[1] MARTIN PRINZ,[3] JAMES J. PAPIKE,[2] and LAWRENCE A. TAYLOR[1]

[1]Planetary Geosciences Institute, Department of Geological Sciences, University of Tennessee, Knoxville, TN 37996
[2]Institute of Meteoritics, Department of Earth and Planetary Sciences, University of New Mexico, Albuquerque, NM 87131
[3]Department of Earth and Planetary Sciences, American Museum of Natural History, New York, NY 10024

(*Received November* 2, 1998; *accepted in revised form May* 20, 1999)

Abstract—The Weekeroo Station IIE iron meteorite contains a variety of felsic and mafic inclusions enclosed in an FeNi-metal host. Petrographic, EMP, and SIMS data suggest that the petrogenesis of the silicates was complex, and included differentiation, remelting, FeO-reduction, and dynamic mixing of phases.

Differentiation produced a variety of olivine-free inclusion assemblages, ranging from pyroxene + plagioclase + tridymite with peritectic compositions, to coarse orthopyroxene, to plagioclase + tridymite and its glassy equivalent. Individual phases have similar trace-element abundances and patterns, despite large variations in inclusion textures, modes, and bulk compositions, probably as a result of mechanical separation of pre-existing phases in an impact event that *dynamically mixed* silicates with the metallic host. Trace-element data imply that augite and plagioclase grains in different inclusions crystallized from the same precursor melt, characterized by relatively unfractionated REE abundances of ~20–30 × CI-chondrites except for a negative Eu anomaly. Such a precursor melt could have been produced by ~2–5% equilibrium partial melting of an H-chondrite silicate protolith, or by higher degrees of partial melting involving subsequent fractional crystallization. Glass appears to have formed by the *remelting* of pre-existing plagioclase and orthopyroxene, in a process that involved either disequilibrium or substantial melting of these phases. During remelting, silicate melt reacted with the FeNi-metal host, and FeO was *reduced* to Fe-metal. Following remelting and metal-silicate mixing, inclusions apparently cooled at different rates in a near-surface setting on the parent body; glass- or pigeonite-bearing inclusions cooled more rapidly (≥2.5°C/hr between 1000–850°C) than pigeonite-free, largely crystalline inclusions.

The results of this study point to two likely models for forming IIE iron meteorites, both involving collision between an FeNi-metal impactor and either a differentiated or undifferentiated silicate-rich target of H-chondrite affinity. Each model has difficulties and it is possible that both are required to explain the diverse IIE group. *Copyright © 1999 Elsevier Science Ltd*

1. INTRODUCTION

Iron meteorites, which consist largely of high-density FeNi-metal and may represent the cores of differentiated asteroids, seem an unlikely rock type in which to find chemically evolved, low-density silicate inclusions. Yet this is precisely the situation for IIE iron meteorites, raising the question of how such fundamentally different materials formed and became juxtaposed. IIE irons are distinguished both by their silicates, which have oxygen-isotopic compositions similar to H-group chondrites (Clayton et al., 1983; Clayton and Mayeda, 1996), and by the chemical composition of the FeNi-metal host (Scott and Wasson, 1976; Wasson and Wang, 1986; Ebihara et al., 1997). Nonetheless, these meteorites are diverse and contain different types of silicate inclusions and variable metallographic textures (e.g., Buchwald, 1975; Prinz et al., 1983; Olsen et al., 1994; Ikeda et al., 1997a).

Variations in silicate inclusion types from one meteorite to another may be especially significant, as they appear to record various stages in the heating, melting, and differentiation of chondritic material. Most inclusions in IIE meteorites have igneous textures and were melted, but some inclusions in Netschaëvo and Techado preserve chondritic textures and were not significantly melted (Olsen and Jarosewich, 1971; Casanova et al., 1995). Silicates in the unclassified meteorite Yamato-791093 may be another example of such largely unmelted material (Ikeda et al., 1997b). The mineralogies and chemical compositions of the inclusions vary widely, ranging from approximately chondritic in Netschaëvo, Techado, and Watson (Olsen and Jarosewich, 1971; Olsen et al., 1994; Casanova et al., 1995), to distinctly non-chondritic in Weekeroo Station, Colomera, Elga, Kodaïkanal, and Miles (Wasserburg et al., 1968; Bunch and Olsen, 1968; Bence and Burnett, 1968; Bunch et al., 1970; Olsen and Jarosewich, 1970; Prinz et al., 1983; Ikeda and Prinz, 1996). The iron meteorites Guin and Sombrerete contain silicate inclusions with fractionated (non-chondritic) compositions reminiscent of those in IIE meteorites, but the silicates in these irons have distinctly different oxygen-isotope compositions, and appear to have been derived from 2 additional, separate parent bodies (Mayeda and Clayton, 1980; Prinz et al., 1983; Rubin et al., 1986).

IIE-like meteorites with silicate inclusions of the fractionated type contain variable amounts of pyroxene, plagioclase, K-feldspar, glass, tridymite, phosphate (e.g., Prinz et al., 1983), and have 2 end-member textural types, cryptocrystalline, and coarse-grained or "gabbroic" (McCoy, 1985; Ikeda and Prinz, 1996). Noteworthy features of these meteorites are the absence

*Author to whom correspondence should be addressed (aruzicka@utk.edu).
†Deceased.

or only small quantity of olivine in them (e.g., Prinz et al., 1983) and the presence in Colomera of one sanidine crystal several cm across (Wasserburg et al., 1968; Takeda et al., 1998). Although there is widespread agreement that the fractionated inclusions were derived from chondritic material by igneous differentiation, the melting mechanism and details of the fractionation process remain unclear. Melting and differentiation may have been triggered by impact processes near the surface of the parent body (Wasson and Wang, 1986; Rubin et al., 1986; Olsen et al., 1994), or by a combination of internal heating within the parent body and shock-melting (Armstrong et al., 1990; McCoy, 1995; Ikeda and Prinz, 1996). In particular, it has been suggested that the coarse-grained inclusions formed by early igneous differentiation (McCoy, 1995; Ikeda and Prinz, 1996), perhaps associated with core-mantle formation in the parent body, whereas the cryptocrystalline inclusions may have formed by later shock-melting (Armstrong et al., 1990; Prinz et al., 1983; McCoy, 1995; Ikeda and Prinz, 1996).

In this study, we use petrographic, electron microprobe (EMP), and secondary-ion-mass-spectrometry (SIMS) techniques to re-examine the petrology of silicate inclusions in the Weekeroo Station IIE iron meteorite. Weekeroo Station (hereafter, WS) was selected for detailed study as it contains a variety of fractionated silicate inclusions (Bunch et al., 1970; Evensen et al., 1979). Olsen and Jarosewich (1970) chemically analyzed a silicate separate from WS, and found that the composition of the separate was similar to that expected for the removal of ~50% olivine (Fo_{80}) from an H-group chondrite. Evensen et al. (1979) found highly variable and fractionated bulk rare-earth-element (REE) patterns for 5 inclusions separated from WS (including splits of some of the same inclusions investigated here), and suggested that the inclusions could have been derived from a single parental melt that was highly evolved and fractionated compared to chondritic material, but which had a time-integrated Rb/Sr ratio at ~4.39 Ga within error of the average chondrite value.

A companion paper (Snyder et al., 1999) discusses Sm-Nd, Rb-Sr, and Hf-W isotope systematics in selected inclusions from Weekeroo Station (including 2 from this study, WSA and WSB), Miles, and Watson.

2. EXPERIMENTAL

An electron microprobe (Cameca SX-50) in the Department of Geological Sciences, University of Tennessee, was used for quantitative phase analyses, X-ray mapping, and for imaging in backscattered-electrons (BSE). Quantitative phase analyses were obtained with the microprobe (operating voltage 15 keV) by using wavelength-dispersive techniques. The beam size and sample current were varied according to the phase being analyzed, to optimize counting statistics and minimize beam-induced element mobilization. For most phases, a focussed (~1-μm-diameter) beam and a 30 na sample current gave good results. For analyses of feldspar and glasses, the beam was expanded (to ~10 μm in diameter) and the sample current was lowered to 10 na. In analyzing lamellar pyroxenes and fine-grained phases, BSE imaging was used to precisely locate individual analyses to minimize beam overlap with surrounding phases. Analyses were deemed acceptable if the analysis total ranged between 98–101 wt%; most analysis totals were between 98.5–100.5 wt%. Modal analyses of the objects were obtained with the microprobe using a digital X-ray mapping technique (Ruzicka et al., 1998), except for inclusion WS2, which consists of glass only, and for WS4, in which areal proportions of the major phases were visually estimated. Areal abundances obtained by X-ray mapping were normalized to 100% after excluding unclassified areas (such as voids) and were assumed to be equivalent to volumetric abundances. The reproducibility of the modal data is estimated as ~5% of the amount of phase present in most cases, although an error of ~20% was assumed for orthopyroxene and pigeonite in objects that contain both these phases. These data were combined with quantitative phase composition data to calculate the bulk compositions of the inclusions. In calculating bulk compositions, the following densities (in g/cm^3) were assumed for different phases: 2.4 (glass), 2.7 (feldspar), 2.3 (tridymite), 3.4 (pigeonite), 3.4–3.5 (orthopyroxene), 3.3 (augite), 4.7 (ilmenite), 5.1 (chromite), 4.6 (troilite), 7.9 (metal), and 3.2 (phosphate). The precision of the calculated bulk weight fractions for different chemical oxides is estimated as ~5% (relative), based on propagation of errors assuming a precision for phase compositions corresponding to the standard deviation ($\pm 1\ \sigma$) of the mean compositions of the major analyzed phases, and the estimated reproducibility of the modal data (see above). Trace-element data for orthopyroxene, augite, plagioclase, and glass were obtained with secondary-ion-mass-spectrometry (SIMS) using a Cameca IMS 4f instrument operated by the University of New Mexico, Albuquerque, and Sandia National Laboratories. Clinopyroxene, orthopyroxene, and glass were analyzed for the rare-earth-elements (REE) La, Ce, Nd, Sm, Eu, Dy, Er and Yb, and also for Sr, Y, and Zr. Plagioclase was analyzed for the same REE and for Sr, Y, and Ba. Samples were bombarded with primary O^- ions, using a current of 30–40 nA and an acceleration voltage of 10 kV. The primary beam diameter on the sample was ~25–35 μm. Secondary ions sputtered from the samples were energy filtered using an energy window of ± 25 V and a sample offset of -75 V. Analyses involved repeated cycles of counting on $^{30}Si^+$, $^{88}Sr^+$, $^{89}Y^+$, $^{137}Ba^+$, $^{90}Zr^+$, $^{139}La^+$, $^{140}Ce^+$, $^{146}Nd^+$, $^{147}Sm^+$, $^{151}Eu^+$, $^{153}Eu^+$, $^{163}Dy^+$, $^{167}Er^+$, $^{174}Zr^+$, as well as counting on a background position. Analytical precision is typically better than 5–10% at concentrations of $1 \times$ CI-chondrites. Absolute concentrations of each element were determined based on empirical relationships between measured peak/$^{30}Si^+$ ratios, normalized to an SiO_2 content determined by prior EMP analysis and to pyroxene, glass, and plagioclase standards.

3. MINERALOGY, TEXTURES, AND MODES

The inclusions in Weekeroo Station vary greatly in mineralogy and texture. Tables 1 and 2 summarize petrographic and modal data for the inclusions, and Fig. 1 illustrates representative textures. For discussion purposes, inclusions are subdivided into 4 textural-mineralogical types:

1. glass-rich inclusions
2. crystalline felsic inclusions
3. crystalline mafic inclusions, and
4. coarse-pyroxene-bearing inclusions.

3.1. Glass-rich Inclusions (WS 2, 7, A)

Glass-rich inclusions contain Si-rich glass either throughout (WS2), or in the mesostases of the inclusions, interstitial to pyroxene grains (WS7, WSA) (Fig. 1a). In both WS7 and WSA, the glass is locally devitrified and cryptocrystalline (grain size <1–5 μm), whereas it is optically isotropic in WS2, aside from one area that has a brown stain and perlitic structure. This area appears to have experienced terrestrial weathering. In both WS7 and WSA, pyroxene grains have euhedral, subhedral, or anhedral outlines and consist primarily of augite that contains exsolution lamellae of low-Ca pyroxene. Judging from EMP data, the dominant low-Ca pyroxene in WS7 is orthopyroxene, whereas both orthopyroxene and pigeonite are present in WSA (Table 2). Some of the pyroxene in WS7 is skeletal. Both WS7 and WSA contain chromite bands or necklaces (typically ~50 μm thick) along the margins of the inclusions. In WS7, a ~2-mm-thick wedge of troilite occurs between the

Table 1. Petrographic data for silicate inclusions in Weekeroo Station.

WS incl.[‡]	Type*	Diameter (mm)[¶]	Predominant mineralogy & texture[§]
A	Glass-rich	31 × ~3	Px set in glass; chr + FeS band at margin
2	Glass-rich	>5 × >3.5	Glass
7	Glass-rich	8 × 4	Px set in glass; chr + FeS band at margin
1A	Crystalline felsic	>8 × >4	Fine-grained radiating plag + trid + FeS
10B	Crystalline felsic	4 × 2	Fine-grained radiating plag + trid
B	Crystalline mafic	25 × ~2.5	Px set in plag + trid mesostasis
1B	Crystalline mafic	>7 × >3	Fine-grained granular plag + trid + px + FeS
5A	Crystalline mafic	7 × 4	Px with interstitial plag + trid; coarse chr
5B	Crystalline mafic	>10 × 4.5	Px with interstitial plag + trid
6	Crystalline mafic	7 × 3	Px with interstitial plag + trid
8A	Crystalline mafic	>5 × >3	Px with interstitial plag + trid
8B	Crystalline mafic	>2.5	Similar to 8A
8C	Crystalline mafic	>7 × >3	Similar to 8A
4	Coarse px-bearing	>6	Coarse opx (single grain) + plag + FeS
10A	Coarse px-bearing	7 × ~2	Coarse px (single grain) + plag + trid

[‡] WS A and WS B were excavated from slab AMNH 2620; the remaining objects were studied in polished thin sections AMNH 2620-1, -2, -4, -5, -6, -7, -8, and -10 (object numbers correspond to last digit of section numbers). Objects 8A, 8B, and 8C are probably fragments of the same object, separated during sectioning; WS 5B and 6 were originally connected in the third dimension (Evensen et al., 1979).

* See text.

[¶] Approximate diameters measured in slab surfaces (A & B) or thin sections; lower limits indicate that inclusions were truncated by section edges.

[§] px = lamellar intergrowths of augite with orthopyroxene or pigeonite; opx = orthopyroxene; plag = plagioclase (oligioclase); trid = tridymite; FeS = troilite; chr = chromite.

chromite band and the host metal in one end of the inclusion; vesicles in WS7 were noted by Evensen et al. (1979). Elongate pyroxene grains in WS7 are preferentially aligned parallel to the long dimension of the inclusion (Fig. 1a). Such an alignment implies the existence of a stress or flow field.

3.2. Crystalline Felsic Inclusions (WS 1A, 10B)

Inclusions 1A and 10B are milky-white megascopically and consist primarily of fine-grained (<50–100 μm) radiating, spherulitic, or granular plagioclase and tridymite (Fig. 1c). Some acicular plagioclase grains are up to 400 μm long. Little pyroxene is present, whereas abundant sulfide occurs in WS1A (Table 2), mainly near the center of the inclusion. Based on their fine grain size and felsic compositions, these inclusions may correspond to the cryptocrystalline inclusions identified in other IIE irons (McCoy, 1995; Ikeda and Prinz, 1996). Along the margins of the inclusions, tridymite grains project into the surrounding metal. This texture implies that the surrounding metal host was at least partly molten during the crystallization of the inclusions, as suggested by Takeda et al. (1998) based on similar textural evidence.

3.3. Crystalline Mafic Inclusions (WS 5A, 5B, 6, 8A–C, B, 1B)

Crystalline mafic inclusions contain lamellar pyroxene grains with interstitial plagioclase and tridymite (Fig. 1b). These inclusions contain only a small amount of glass (WSB) or are holocrystalline. Textures in them vary from granular and fine-grained (<100 μm), as in WS1B, to coarser-grained and more microporphyritic (with pyroxene grains typically ~40–400 μm across) in the other inclusions. In the latter, the shapes of pyroxene grains vary from tabular, to rounded, to irregular.

Table 2. Modal compositions (vol%) of silicate inclusions in Weekeroo Station.

WS incl.	*A*	*2*	*7*	*1A*	*B*	*1B*	*5A*	*5B*	*6*	*4*
	Glass-rich			Crys. felsic	Crystalline mafic					Coarse px
Orthopyroxene	5.4	—	6.2	1.0	15.3	15.7	26.6	21.3	14.1	90.7
Augite	29.7	—	36.0	1.4	13.2	21.6	10.8	18.8	25.7	—
Pigeonite	2.7	—	—	—	9.8	—	—	—	—	2.8
Plagioclase	—	—	—	66.1	55.7	44.3	43.8	47.5	51.3	3.9
K-feldspar	<0.1	—	0.2	0.2	0.2	1.3	0.4	0.4	0.3	—
Tridymite	—	—	0.6	18.2	3.4	6.9	10.1	10.9	7.8	—
Glass	59.3	100	55.1	—	—	—	—	—	—	—
Ilmenite	0.2	—	<0.1	0.7	<0.1	0.1	0.1	<0.1	<0.1	—
Chromite	0.7	—	0.6	0.2	0.1	0.3	5.3	0.1	0.1	—
Troilite	0.6	—	0.5	11.0	0.7	9.2	2.4	0.5	0.1	2.6
Kamacite	0.6	—	0.6	0.8	0.7	0.3	0.1	0.1	0.1	—
Phosphate*	0.8	—	0.2	0.4	0.9	0.5	0.4	0.4	0.5	—

* Includes both merrillite and apatite.

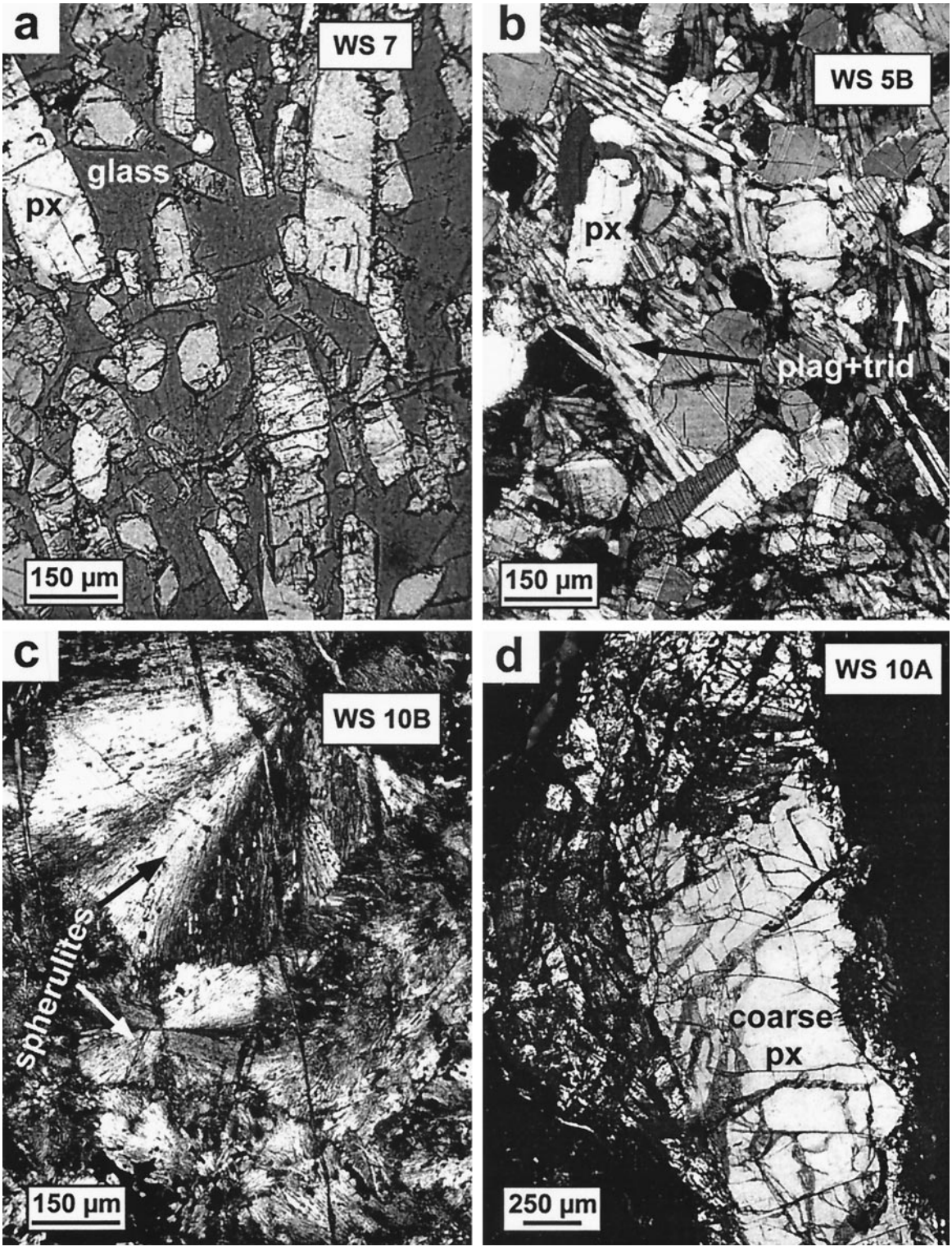

Fig. 1. Micrographs of silicate inclusions in Weekeroo Station obtained in plane-polarized (a,d) and cross-polarized transmitted light (b,c). (a) WS7, showing tabular pyroxene phenocrysts (mainly augite) set in glass. Pyroxene grains are mainly euhedral and have a preferred orientation parallel to the long dimension of the inclusion (oriented top-bottom). (b) WS5B, showing tabular and equant pyroxene grains with exsolution lamellae set in a holocrystalline groundmass containing acicular-to-tabular plagioclase grains and tridymite. Pyroxene grains have rounded or irregular margins. (c) WS10B, showing spherulitic texture of fine-grained plagioclase and tridymite. (d) WS10A, showing a portion of an anomalously coarse (~4 × 1 mm-wide) pxyoxene grain with irregular edges, enclosed in a fine-grained groundmass consisting mainly of plagioclase and tridymite.

Pyroxene grains are commonly present in clusters, and are sometimes twinned and often lamellar. Lamellar pyroxenes consist either of augite hosts with orthopyroxene lamellae, or vice versa; lamellae spacings vary from grain-to-grain and within grains. As in WS7, pyroxene grains are preferentially aligned in WS5B (parallel to the long dimension of the inclusion), in WS8A–C (which probably represent a single inclusion that was sectioned into 3 pieces), and locally within WS5A. Plagioclase grains are typically less than 40 μm wide, and some acicular grains can be up to 600 μm long. Coarse-grained ($\sim$0.2–0.5 mm), euhedral-subhedral chromite is concentrated along the margins of WS5A, and phosphate minerals (both merrillite and apatite) are concentrated on the margins of some of the inclusions.

Inclusions of this type appear to correspond to the coarse-grained (McCoy, 1995) or gabbroic inclusions (Ikeda and Prinz, 1996; Ikeda et al., 1997a) identified in other IIE irons. However, in WS the tridymite and exsolved pyroxene grains are more common than in Miles (Ikeda and Prinz, 1996; Ikeda et al., 1997a).

Some of these inclusions exhibit significant textural heterogeneities and contain features that resemble those found in other inclusion types. WSB has regions nearly devoid of pyroxene grains; these contain radiating intergrowths of plagioclase and tridymite similar to that observed in WS 1A and 10B. As with the latter inclusions, tridymite grains along the margin of WSB project into the surrounding metal host. Two unusually coarse, lamellar, tabular pyroxene grains (1 mm and 0.8 mm long, respectively) are present in WS5A, reminiscent of coarse pyroxene found in WS10A (see below).

3.4. Coarse-pyroxene-bearing Inclusions (WS 4, 10A)

Inclusions WS4 and 10A contain unusually coarse pyroxene grains that may correspond to the "coarse-grained" inclusions in IIE irons identified by McCoy (1995). WS4 is dominated by a single coarse (>3–5 mm wide) crystal of orthopyroxene that has weak undulose extinction. Pigeonite blebs occur along the rim of this crystal. Fine-grained (<100 μm) plagioclase, troilite, chromite, and tridymite occur along one margin of the inclusion. Inclusion WS4 is truncated by the section edge, but the orthopyroxene crystal it contains was reported by Evensen et al. (1979) to be 7 mm wide before sectioning. WS10A contains one irregularly-shaped, coarse ($\sim 4 \times 1$ mm) lamellar pyroxene grain enclosed by fine-grained (<50–100 μm) radiating plagioclase and tridymite (Fig. 1d). The groundmass of WS10A resembles that of WS1A and nearby WS10B (see above). The large pyroxene is aligned parallel to the long dimension of the inclusion. No corona of orthopyroxene surrounds this lamellar pyroxene, as has been reported for large augite grains elsewhere in Weekeroo Station (Bunch et al., 1970), Miles (Ikeda and Prinz, 1996; Ikeda et al., 1997a), Guin (Rubin et al., 1986), and Colomera (Takeda et al., 1998).

The anomalously large size of pyroxene grains in these inclusions and in WS5A suggest that the grains may be xenocrysts, in the sense of not having crystallized together with the remainder of the inclusions. The irregular margin of the coarse pyroxene in WS10A (Fig. 1d) may indicate that it experienced mechanical abrasion. Consequently, physical mixing may have been involved in the formation of these inclusions. Such a mixing process is consistent with the stress or flow field inferred from the preferential alignment of pyroxene grains in some inclusions.

4. MAJOR-ELEMENT PHASE COMPOSITIONS

Representative microprobe analyses of the major phases found in the inclusions, pyroxene, plagioclase, tridymite, and glass, are given in Table 3. These data are discussed for each phase separately below.

4.1. Pyroxene

Silicate inclusions in Weekeroo Station contain augite ($Wo_{32.9-43.4}En_{40.9-48.8}Fs_{11.9-21.9}$), orthopyroxene ($Wo_{1.1-5.1}En_{56.3-79.0}Fs_{18.0-40.9}$), and less commonly, pigeonite ($Wo_{5.2-10.7}En_{57.9-67.0}Fs_{25.6-34.5}$). Grain core-to-rim variations in composition were not observed, except for the coarse orthopyroxene grain in WS4, which has normal zoning in Fe-Mg, a uniform Ca content throughout much of its interior, and a Ca-poor rim zone (Fig. 2; Table 3a). The very edge of the large orthopyroxene is iron-poor (Fig. 2), especially close to the FeNi-metal host.

The presence of 2 or 3 pyroxene polymorphs, which contain generally low abundances of minor elements (Table 3a), and which presumably formed under conditions of low pressure, make these inclusions well-suited for pyroxene geothermometry. Fig. 3 shows compositions projected on the pyroxene graphical thermometer (Lindsley and Andersen, 1983), including contours of apparent equilibration temperatures, and equilibrium tie-lines between illustrative sets of co-existing pyroxene polymorphs.

From Fig. 3, it is immediately obvious that, in some cases, orthopyroxene is not in equilibrium with coexisting augite or pigeonite, despite the fact that most of the orthopyroxene and augite analyses represent host-lamella pairs that presumably formed in equilibrium during exsolution. Disequilibrium is implied by the large variations in Fe/Mg (Fs/En) for orthopyroxene, in contrast to the situation for augite and pigeonite, which have more restricted compositions (Fig. 3). Inclusions 5A, 5B, 6 and 7 contain orthopyroxene that is too ferrous to be in equilibrium with co-existing pigeonite or augite, whereas some orthopyroxene in inclusions 4 and 7 is too magnesian to be in equilibrium with co-existing pigeonite or augite (Fig. 3).

Disequilibrium is also implied by the tendency for orthopyroxene to yield lower apparent equilibration temperatures than for co-existing augite and pigeonite (Fig. 3, 4). Apparent equilibration temperatures are $\sim$950–1150°C for augite and pigeonite, and $\sim$700–1000°C for orthopyroxene, except for coarse orthopyroxene in WS4 (Fig. 2). The latter yields high apparent equilibration temperatures ($\sim$1080°C) in the grain core, similar to that of augite and pigeonite in other inclusions, and low temperatures ($\sim$800°C) in the grain rim, similar to that of fine-grained orthopyroxene in other inclusions (Fig. 2, 4).

These data suggest that the relatively fine-grained augite and pigeonite, and the core of the coarse orthopyroxene grain, record high-temperature equilibration, during either cooling from magmatic temperatures or during a secondary partial melting event. The fine-grained orthopyroxene and the rim of the coarse orthopyroxene may have reacted with their sur-

Table 3a. Representative major-element abundances in pyroxene.

WS inclusion phase*	(1) *A* aug	(2) *A* pig	(3) *A* opx aj chr	(4) *7* aug	(5) *7* opx	(6) *7* opx aj Fe	(7) *4* opx core	(8) *4* opx rim	(9) *4* opx aj Fe	(10) *1B* aug	(11) *1B* opx	(12) *6* aug lam	(13) *6* opx host	(14) *5A* aug lam	(15) *5A* opx host
wt%															
SiO_2	52.2	52.9	54.5	52.6	52.9	55.8	55.9	54.0	55.9	52.4	53.6	52.1	52.2	53.0	53.0
TiO_2	0.41	0.41	0.29	0.47	0.12	0.31	0.05	0.08	0.20	0.52	0.26	0.49	0.28	0.23	0.11
Al_2O_3	1.28	0.21	0.30	1.88	0.49	1.26	0.28	0.29	0.20	0.81	0.16	0.90	0.21	1.14	0.41
Cr_2O_3	0.90	0.26	0.72	0.84	0.33	0.71	0.61	0.31	0.19	0.93	0.16	1.00	0.22	1.38	0.46
FeO	10.2	19.2	13.7	8.56	21.51	12.1	11.7	18.5	12.7	10.7	17.0	9.10	22.78	7.90	20.9
MnO	0.83	1.45	1.18	0.65	1.42	1.07	0.50	1.14	1.18	1.01	1.46	0.66	1.44	0.62	1.47
MgO	15.1	21.2	27.8	15.1	21.8	27.8	29.7	24.8	29.5	15.6	25.3	14.5	20.6	14.9	22.5
CaO	17.8	3.56	0.55	19.5	1.29	0.64	1.57	0.98	0.58	16.8	1.10	20.0	1.27	20.2	0.74
Na_2O	0.44	0.06	<0.03	0.42	0.04	0.44	0.03	0.03	<0.03	0.44	<0.03	0.56	0.03	0.61	0.02
	99.2	99.2	99.2	100.0	99.9	100.2	100.4	100.0	100.5	99.1	99.1	99.4	99.0	100.0	99.6
mol%**															
Wo	37.6	7.2	1.1	40.9	2.6	1.3	3.0	1.9	1.1	35.2	2.2	41.8	2.6	42.4	1.5
En	44.3	60.0	76.0	44.1	61.2	78.0	78.8	67.9	78.2	45.6	69.4	42.3	58.6	43.6	63.2
Fs	18.1	32.8	22.9	15.1	36.2	20.7	18.2	30.2	20.7	19.2	28.4	15.9	38.8	14.0	35.3
Teq (°C)†	1110	1095	725	1050	850	780	1050	800	750	1150	850	950	820	1050	700

* Aug = augite; pig = pigeonite; opx = orthopyroxene; lam, host = lamellae & host pairs; aj Fe = adjacent Fe-Ni-metal host; aj chr = adjacent chromite necklace surrounding inclusion.

** Wo = 100 Ca/[Mg + Fe + Ca]; En = 100 Mg/[Mg + Fe + Ca]; Fs = 100 Fe/[Mg + Fe + Ca].

† Approximate equilibration temperature, based on Lindsley and Andersen (1983) geothermometer.

roundings at a lower temperature, although it is also possible to interpret the low apparent temperatures for such orthopyroxene as "minimum temperatures" that do not reflect 2-pyroxene or 3-pyroxene equilibrium (Lindsley and Andersen, 1983).

Orthopyroxene analyses show two trends on an FeO-MnO plot (Fig. 5). Trend 1, which is best observed for the core of the large orthopyroxene grain in inclusion 4, involves a simple positive correlation between FeO and MnO, consistent with igneous fractionation alone. Trend 2 also involves an overall correlation between FeO and MnO, but it is displaced to lower FeO/MnO values, and it appears to be curved (Fig. 5). Orthopyroxene grains closest to the FeNi-metal host belong to Trend 2 and have the lowest FeO contents and lowest FeO/MnO values. This implies that these grains may have reacted with the host, losing FeO in a reduction process. However, FeO-reduction alone cannot explain the tendency for Trend 2 orthopyroxene grains to have *co-varying* FeO and MnO abundances. This may indicate that Trend 2 was established by the simultaneous igneous fractionation and FeO-reduction of a silicate melt. Orthopyroxenes that crystallized from such a melt would tend to show a positive correlation between FeO and MnO established by normal igneous partitioning, but would have variable

Table 3b. Representative major-element abundances in feldspar and tridymite.

WS inclusion phase*	(1) *1A* plag	(2) *1B* plag	(3) *4* plag	(4) *5B* plag	(5) *1A* trid	(6) *5A* trid
wt%						
SiO_2	64.6	63.8	64.2	64.8	97.3	96.5
TiO_2	0.10	0.06	0.08	0.09	0.23	0.51
Al_2O_3	22.0	21.9	21.8	21.8	1.31	1.77
Cr_2O_3	<0.03	0.06	0.03	<0.03	<0.03	<0.03
FeO	0.40	0.29	0.66	0.15	0.16	0.12
MnO	0.04	<0.03	<0.03	<0.03	<0.03	<0.03
MgO	<0.03	<0.03	0.25	<0.03	<0.03	<0.03
CaO	3.08	3.21	3.25	2.80	0.04	0.27
Na_2O	9.16	9.32	9.24	9.44	0.39	0.53
K_2O	0.93	0.67	0.64	0.81	0.41	<0.03
	100.3	99.4	100.0	99.8	99.8	99.7
mol%**						
Ab	79.9	80.8	80.7	81.9		
Or	5.3	3.9	3.7	4.6		
An	14.8	15.4	15.7	13.4		

* plag = plagioclase; trid = tridymite.

** Ab = 100 Na/[Na + K + Ca]; Or = 100 K/[Na + K + Ca]; An = 100 Ca/[Na + K + Ca].

Table 3c. Representative major-element abundances in glasses.

WS inclusion	(1) *2*	(2) *A*	(3) *7*	(4) *7* Si-rich	(5) *7* K-rich	(6) *rhyolite* †	(7) *tektite* §
wt%							
SiO_2	79.8	73.8	73.8	84.6	72.9	73.2	62–80
TiO_2	0.21	n.a.	0.21	0.15	0.19	0.2	0.49–1.0
Al_2O_3	11.7	16.2	15.7	9.21	15.2	14	8.9–18
Cr_2O_3	<0.03	n.a.	0.05	<0.03	0.11	—	—
FeO*	0.13	0.11	0.10	0.48	0.61	2.2	3.6–8.6
MnO	0.05	n.a.	<0.03	<0.03	<0.03	—	—
MgO	1.00	<0.03	<0.03	<0.03	0.49	0.4	1.3–8.0
CaO	1.72	2.09	1.33	0.82	1.29	1.3	1.4–9.8
Na_2O	4.69	7.18	7.51	4.26	5.03	3.9	0.62–3.9
K_2O	0.53	0.71	1.10	0.47	4.56	4.1	0.90–2.8
	99.8	100.1	99.9	100.0	100.4	99.3	
Normative minerals (mol%)**							
Or	1.20	2.17	3.50	0.91	14.74	11.45	
Ab	15.99	33.26	36.66	12.58	24.75	16.55	
An	3.24	5.14	3.55	1.35	3.49	3.05	
Cpx	0.00	0.19	0.00	0.00	0.00	0.00	
Wo	0.00	0.00	0.00	0.00	0.00	0.00	
Opx	2.93	0.01	1.81	0.69	2.68	2.18	
Qz	76.35	59.23	54.49	84.29	54.34	65.76	
Cor	0.29	0.00	0.00	0.18	0.00	1.02	

† typical rhyolite (McBirney, 1993).
§ compositional range for Australasian tektites (Koeberl, 1986).
* all iron as FeO.
** Or = $KAlSi_3O_8$, Ab = $NaAlSi_3O_8$, An = $CaAl_2Si_2O_8$, Cpx = $Ca(Mg, Fe)Si_2O_6$, Wo = $CaSiO_3$, Opx = $(Mg, Fe)_2Si_2O_6$, Qz = SiO_2, Cor = Al_2O_3. n.a. = not analyzed.

FeO/MnO ratios depending on the extent of FeO-reduction and their proximity to the FeNi-metal host.

Orthopyroxene grains closest to the FeNi-metal host have low Fs and Wo contents and low apparent equilibration temperatures (~700–800°C) (columns 3, 6, and 9 in Table 3a). At face value, the low temperatures imply subsolidus conditions, but, as noted above, these temperatures strictly represent minimum temperatures only, if the orthopyroxene grains were not in equilibrium with another pyroxene.

4.2. Feldspar and Tridymite

In contrast to orthopyroxene, the major-element composition of feldspar in the inclusions is uniform, corresponding to oligoclase (mainly $Ab_{78-85}Or_{5-8}An_{10-17}$) (Fig. 6, Table 3b). This resembles the composition of plagioclase in type 6 ordinary chondrites. A few analyses of feldspar with up to ~15 mol% Or were obtained (Fig. 6), but otherwise, no K-feldspar sufficiently coarse to analyze quantitatively was found. However, X-ray mapping implies the existence of small K-rich patches that probably correspond to the cryptoperthite that was previously inferred for Weekeroo Station (Bunch and Olsen, 1968).

The uniformity of plagioclase compositions is especially notable considering the overall differences in textures and mineralogies between the inclusions. For example, although WS 1A, 1B, 4 and 5B have drastically different textures and plagioclase/pyroxene ratios (Table 1, 2, and above), their plagioclase compositions are essentially identical (Table 3b). Moreover, plagioclase grain compositions do not appear to be significantly different in inclusions that have clinopyroxene equilibration temperatures that are relatively high (e.g., WS 1A, 1B) and in those that are relatively low (e.g., WS5B) (Table 3b).

Analyses of silica polymorph show elevated contents of Al (Table 3b). This is consistent with the optical identification of the polymorph as tridymite.

4.3. Silica-rich Glasses

Silica-rich glass was identified in four inclusions (WS A, B, 2 and 7), although only minor amounts are present in WSB. Representative compositions of this glass are given in Table 3c, and Fig. 7 shows the composition of glass analyses expressed in normative minerals. Inclusion WS2, which consists entirely of glass, has a rather uniform composition, whereas inclusions WS A, B and 7, which consist of partly-devitrified glass interstitial to pyroxene, contains glass of more variable composition (Fig. 7). All of the glasses can be described as a mixture of normative feldspar and quartz, and more specifically, as a mixture of normative *plagioclase* and quartz (Fig. 7). Normative orthopyroxene (<5 mol%) is the most significant "other" component in the glass (Table 3c).

In general, the glass is rhyolitic or tektite-like in composition, although MgO and FeO abundances are lower, and Na_2O abundances are higher, in the inclusions compared to typical rhyolites or tektites (Table 3c). The overall similarity of the glass to rhyolites suggests that this glass represents a chemically evolved, low-melting-temperature fraction, and supports the previous characterization of some inclusions in IIE irons as rhyolitic (Armstrong et al., 1990) or minimum melts (Prinz et al., 1983).

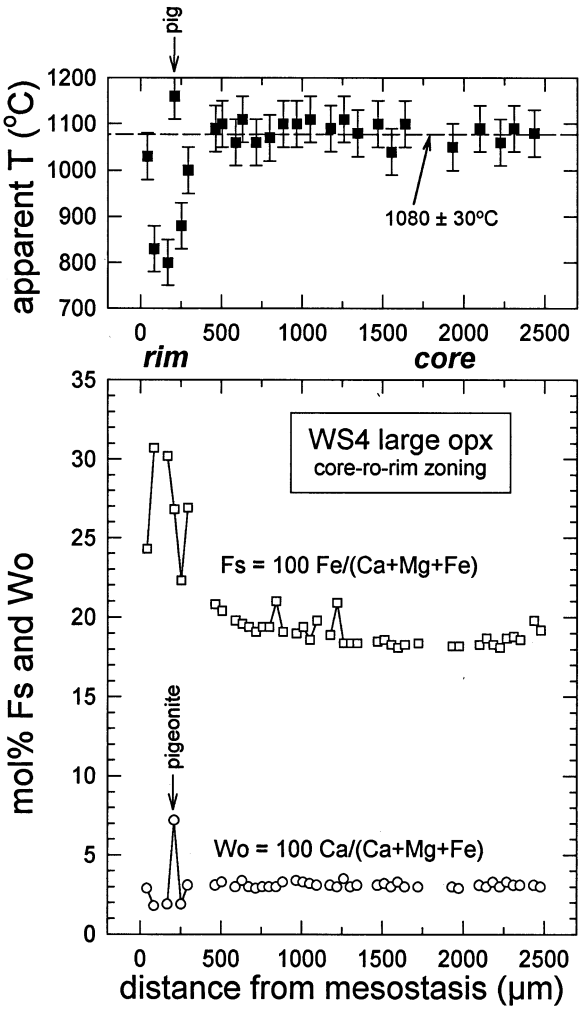

Fig. 2. Variation in the composition of the large orthopyroxene grain in WS4, obtained in a core-to-rim microprobe traverse, and corresponding temperatures based on the Lindsley and Andersen (1983) geothermometer. The orthopyroxene grain shows normal Fe-Mg zoning and uniform Ca content throughout most of its interior, but has a Ca-poor rim. Geothermometry suggests apparent equilibration of the core at a high temperature (~1080°C), and apparent equilibration of the Ca-poor rim at a lower temperature (~800°C).

5. MAJOR-ELEMENT BULK COMPOSITIONS

Major-element bulk compositions of Weekeroo Station inclusions are given in Table 4. For comparison, Appendix 1 provides a compilation of previously-determined major-element compositions for silicate inclusions in IIE-like meteorites. The bulk compositions of IIE silicate inclusions vary greatly (Table 4, Appendix 1), reflecting the diverse modes of the inclusions (Table 2). The compositions of inclusions in Weekeroo Station are generally similar to those in other IIE (and IIE-like) meteorites with fractionated silicates, except that the abundance of alkalis (and especially K_2O) tend to be higher in inclusions from Kodaikanal, Elga, and Colomera (Appendix 1).

Fig. 8 demonstrates that the inclusions in IIE meteorites do not have compositional trends similar to that of terrestrial volcanic rocks. Terrestrial volcanic rocks show a clear inverse correlation between alkali and silicae abundances on the one hand, and Mg# on the other. In contrast, IIE inclusions have a rather restricted variation in Mg# (Ikeda and Prinz, 1996; Ikeda et al., 1997a), despite alkali abundances that vary by a factor of 30 (from ~0.38 wt% in WS4 to ~13 wt%), and silica abundances that vary by a factor of 2 (from ~45–48 wt% in Watson and Netschaëvo, to ~80 wt% in WS2).

Normative compositions of the inclusions are shown in Fig. 9, projected onto the olivine-quartz-plagioclase liquidus diagram of Longhi (1991). The normative compositions of the IIE inclusions scatter widely, do not follow a simple trend, and do not cluster strongly around cotectics or reaction lines and points, although several inclusions from WS do cluster around peritectic R (Fig. 9). Taken as a group, the large scatter and lack of systematic relationships for IIE inclusions suggest that they were not differentiated in the same way as terrestrial volcanic rocks. In particular, their varied compositions appear to reflect processes other than simple partial melting or fractional crystallization.

The WS inclusions that cluster around the peritectic point include inclusions B, 1B, 5A, 5B, and 6; inclusion A may also belong to this cluster. Aside from WSA, these inclusions consist of the "crystalline mafic" type. The peritectic compositions of these inclusions could have formed by simple partial melting of an ordinary chondrite precursor.

6. TRACE-ELEMENT ABUNDANCES

Trace-element abundances for various rare-earth-elements (REE), in addition to Sr, Y, and either Ba or Zr, were obtained by SIMS techniques for pyroxene, plagioclase, and glass. The results are given for each phase separately in Table 5a–c and are shown in chondrite-normalized diagrams in Fig. 10a–c.

The overall abundances of incompatible elements in the various phases are similar to those determined by Hsu et al. (1997) for two inclusions in Colomera, although we did not find evidence for the distinctive Yb anomalies reported by these researchers. Moreover, the overall REE abundances are similar to those found by Evensen et al. (1979) in bulk analyses of WS 1A, 1B, 5A, 6, and 7.

The trace-element data for Weekeroo Station reveal that individual phases in different inclusions have similar trace-element abundances and patterns, despite large variations in textures, modes, and bulk compositions for the inclusions. For example, fine-grained orthopyroxene in inclusion WS1B and coarse-grained orthopyroxene in WS4 have similar trace-element abundances (Fig. 10a). This is in spite of the overall peritectic bulk major-element composition of the former *versus* the highly orthopyroxene-rich composition of the latter, and in spite of the generally more ferrous composition of orthopyroxene in WS1B ($Wo_{1.7–2.8}En_{64.6–70.1}Fs_{27.4–32.6}$) compared to WS4 ($Wo_{1.1–3.8}En_{67.3–79.0}Fs_{18.0–30.7}$). Similarly, trace-element abundances in augite in glass-rich inclusion WS7 are similar to that of augite in glass-poor inclusion WS1B (Fig. 10a). Trace-element patterns in glass from WS2 and WS7 are distinctive, yet similar to one another (Fig. 10c). Finally, trace-element patterns in plagioclase from the crystalline felsic inclusion WS1A are similar to that in the crystalline mafic inclusion WS1B (Fig. 10b).

Chondrite-normalized patterns of glasses in WS2 and WS7

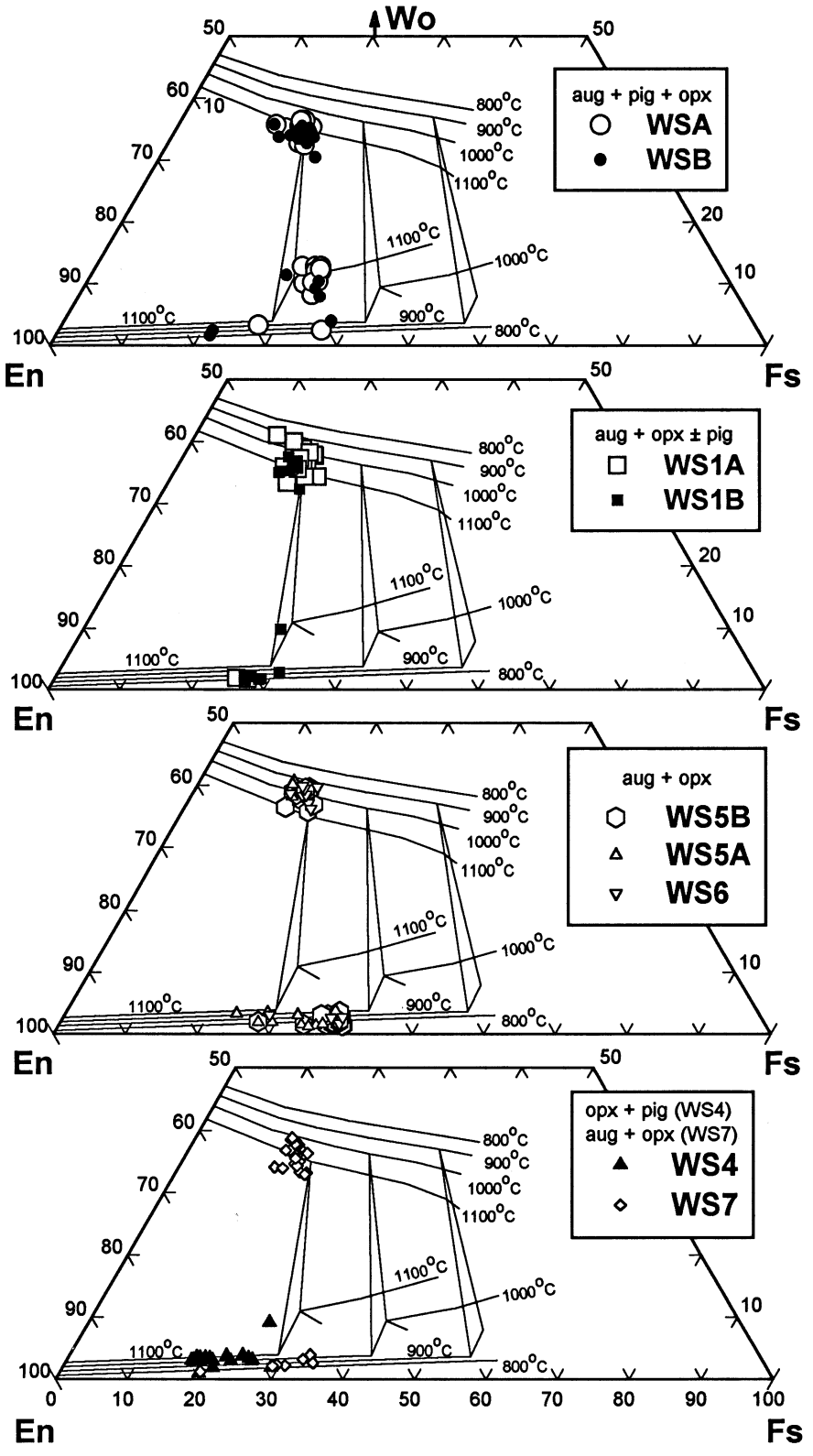

Fig. 3. Pyroxene quadrilateral showing pyroxene compositions in Weekeroo Station, projected using the scheme of Lindsley and Andersen (1983). Isotherms and equilibrium 3-phase triangles are from the latter. For multiple pyroxene polymorphs that are in equilibrium with one another, the isotherms represent equilibration temperatures, whereas for a single pyroxene polymorph that is not in equilibrium with another pyroxene polymorph, the isotherms represent minimum formation temperatures (Lindsley and Andersen, 1983).

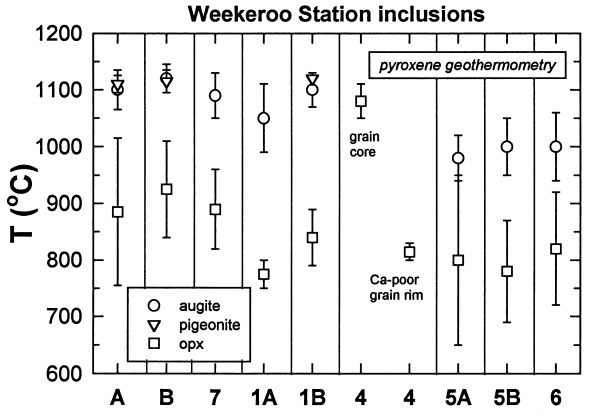

Fig. 4. Summary of apparent equilibration temperatures (mean ± standard deviation) for analyses of pyroxene in Weekeroo Station inclusions, using the Lindsley and Andersen (1983) geothermometer. Equilibration temperatures for augite and pigeonite range from ~1100°C in inclusions A, B, 7 and 1B, to ~1000°C in inclusions 5A, 5B, and 6, with inclusion 1A having intermediate temperatures. These variations may reflect differences in cooling rates from magmatic temperatures. Except for the core of the coarse-grained orthopyroxene grain in WS4, orthopyroxene in the inclusions appears to have equilibrated at lower temperatures (~700–1000°C) than the augite, but this may reflect disequilibrium and represent a "minimum temperature" only.

(Fig. 10c) show large positive Eu anomalies, and complex "concave-downward" patterns for both the HREE and LREE, often featuring high Er/Yb and Er/Dy ratios, and high Nd/Sm and Nd/Ce ratios. The glasses have low overall abundances of incompatible elements, unlike what one might expect of evolved, igneous melts. Yet the major-element compositions of the glasses are evolved (i.e., rhyolitic), and the glass in WS2 is similar to that expected for a eutectic melt composition.

The trace-element data provide striking evidence for disequilibrium between co-existing glass and augite in inclusion WS7. The glass in this inclusion contains lower overall abundances of

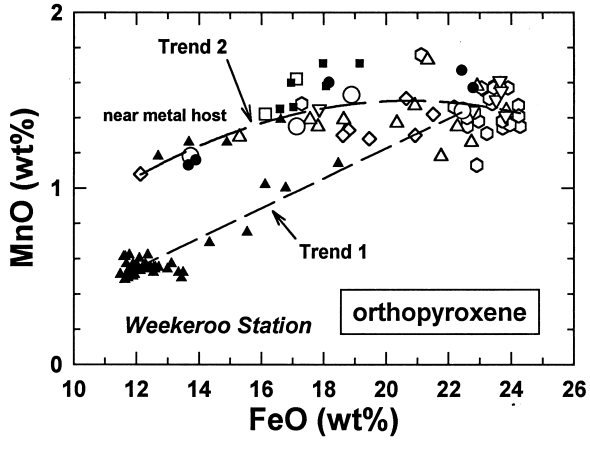

Fig. 5. FeO and MnO abundances in orthopyroxene show two chemical trends, designated Trend 1 and Trend 2. Trend 1 is attributed to igneous fractionation alone; Trend 2 is attributed to a combination of igneous fractionation and FeO-reduction in melts caused by reaction with the metallic host. Symbols correspond to those in Fig. 3. See Text.

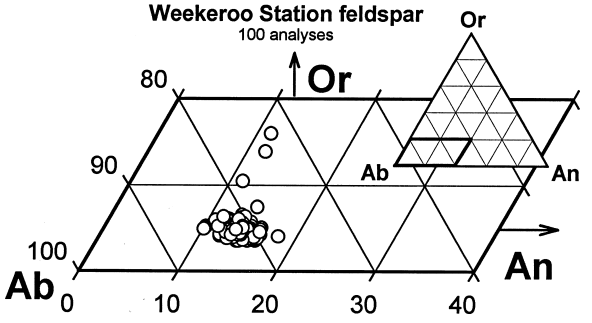

Fig. 6. Feldspar in Weekeroo Station shows limited major-element compositional variability, ranging mainly between An_{10-17}, Or_{5-8}, and Ab_{78-85}. An = Ca/[Ca + Na + K], Ab = Na/[Ca + Na + K], Or = K/[Ca + Na + K] in atomic %.

incompatible elements (except for Eu, Sr, Zr and La) than co-existing augite (Fig. 10a,c). This is unlike what one would expect for mineral-melt partitioning, as incompatible elements should preferentially partition into the remaining melt fraction (which ultimately solidified to glass). The large discrepancy between what is observed in WS7 and what is expected on the basis of augite-melt equilibrium is shown in Fig. 11, based on D-values determined by McKay et al. (1986). Compared to augite-melt equilibrium, the augite is enriched in all of the REE except Eu by a factor of 10–100 (Fig. 11). The apparent good match for Eu is deceptive, as the equilibrium partition coefficient for Eu should probably be lower than for the relatively oxidizing case pertaining in the experiments of McKay et al. (1986). In any case, these data clearly demonstrate that the trace-element abundances of augite and glass in WS7 do not represent equilibrium mineral-melt partitioning.

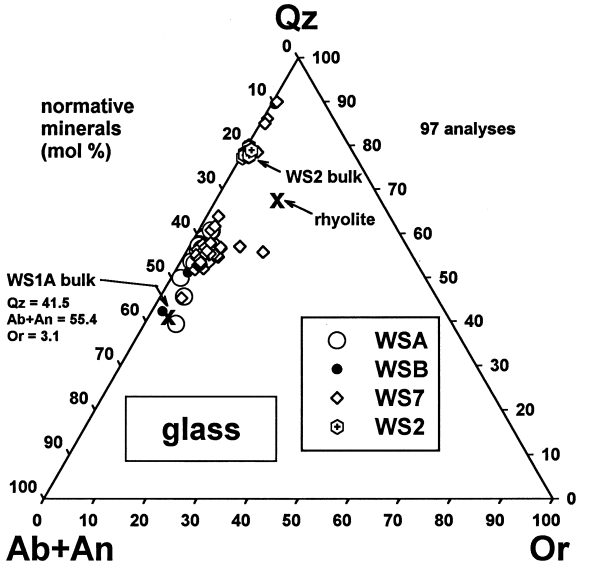

Fig. 7. Ternary diagram illustrating the normative composition of glass in Weekeroo Station compared to terrestrial rhyolite (McBirney, 1993) and holocrystalline inclusion 1A.

Table 4. Major-element bulk compositions of Weekeroo Station inclusions.[†]

WS incl.	*A*	*B*	*1A*	*1B*	*2*	*4*	*5A*	*5B*	*6*	*7*	*avg. ± s.d.*	*tholeiitic andesite*[§]	*icelandite*[§]	*H-chon. silicate*[‡]
wt%														
SiO_2	56.9	58.2	54.9	51.6	79.4	53.5	53.7	60.7	60.6	61.2	59.1 ± 7.5	58.9	61.8	47.80
TiO_2	0.37	0.24	0.79	0.36	0.21	0.06	0.47	0.28	0.33	0.29	0.34 ± 0.18	2.2	1.3	0.20
Al_2O_3	11.8	11.1	13.7	8.91	11.6	0.99	9.38	9.95	10.6	7.78	9.58 ± 3.27	15.5	15.4	3.50
Cr_2O_3	1.01	0.29	0.26	0.52	0.02	0.78	5.29	0.39	0.43	1.05	1.00 ± 1.46	—	—	0.55
FeO	5.74	6.19	1.08	5.53	0.20	11.9	9.65	7.87	6.73	5.85	6.07 ± 3.32	7.9	8.0	12.70
MnO	0.41	0.48	0.07	0.51	0.05	0.59	0.61	0.52	0.47	0.43	0.41 ± 0.19	0.2	—	0.33
MgO	7.26	9.30	0.70	7.92	1.08	26.3	8.95	8.40	7.87	8.59	8.63 ± 6.59	2.7	1.8	31.00
CaO	7.90	5.38	2.45	5.83	1.53	2.07	3.97	5.88	7.16	8.16	5.03 ± 2.30	6.7	5.0	2.32
Na_2O	5.16	4.81	5.73	3.78	4.98	0.36	3.66	4.29	4.66	3.42	4.09 ± 1.42	4.1	4.4	1.13
K_2O	0.50	0.49	0.61	0.47	0.38	0.02	0.38	0.45	0.48	0.64	0.44 ± 0.16	1.1	1.6	0.16
P_2O_5	0.38	0.45	0.20	0.23	—	—	0.19	0.20	0.25	0.10	0.25 ± 0.11	0.4	0.4	0.34
Fe	2.14	2.50	13.1	9.33	—	2.23	2.48	0.74	0.35	2.06	3.88 ± 4.07	—	—	—
Ni	0.11	0.12	0.14	0.05	—	—	0.02	0.02	0.02	0.11	0.07 ± 0.05	—	—	—
S	0.34	0.40	6.33	4.95	—	1.28	1.29	0.28	0.06	0.29	1.69 ± 2.18	—	—	—
atomic														
Mg#	0.69	0.73	0.54	0.72	0.91	0.80	0.62	0.66	0.68	0.72	0.71 ± 0.09	0.38	0.29	0.81

[†] Determined by modal reconstruction, except for WS2 (average of 29 microprobe analyses).
[§] Typical tholeiitic andesite and icelandite (McBirney, 1993).
[‡] Average H-chondrite fall (Jarosewich, 1990). Mg# = $Mg/[Mg + Fe^{2+}]$.

7. DISCUSSION

7.1. Thermal Histories

Various evidence suggests that the inclusions cooled relatively rapidly in a near-surface environment on the parent body and were not significantly affected by high-temperature metamorphism. This includes the presence of glass, spherulitic textures, fine grain sizes, and the high and variable closure temperatures for clinopyroxene.

The presence of silica-rich glass in some inclusions can be used to estimate the cooling rates of these inclusions. As noted above, the glass is broadly similar in composition to that of tektites (Table 3c). Annealing experiments on anhydrous tektite compositions indicate that devitrification occurs rapidly, within 10 h to a few days at temperatures between 1050–800°C (Fig. 12) (Barnes and Russell, 1966; Wosinski et al., 1967). By analogy to tektites, the presence of undevitrified (in WS2) or minimally devitrified (in WS A and 7) glass in the IIE inclusions implies that they must have cooled rapidly from melt temperatures, within ~20 h to 1000°C, and within ~80 h to 850°C (Fig. 12). For the glass-bearing inclusions, this implies a cooling rate of ≥2.5°C/hr over the temperature interval of 1000–850°C. Such a rapid cooling rate is more consistent with a near-surface, impact-melt origin than with deep-seated, planetary differentiation.

The high closure temperatures (1000–1100°C) for augite, pigeonite, and the core of the coarse orthopyroxene grain also suggest rapid cooling at high temperatures. However, the cooling rates do not appear to have been identical for different inclusions. Although augite compositions vary modestly, they appear to correlate with the overall textures and mineralogies of the inclusions, in a fashion consistent with differences in cooling rates. Apparent augite equilibration temperatures are highest (~1100°C) and Wo contents are lower ($Wo_{36.8-38.3}$ on average) for those inclusions that contain glass (WS A, 7), pigeonite (WS A, B, 1B), or are relatively fine-grained (WS 1A, 1B) (Fig. 4). In contrast, equilibration temperatures are lower (~1000°C) and Wo contents are higher ($Wo_{39.0-42.1}$ on average) for augite in inclusions that lack glass and pigeonite and instead contain relatively coarse mesostases (WS 5A, 5B, 6) (Fig. 4). This suggests that the high-temperature cooling rates of inclusions differed, being faster in the glass- or pigeonite-bearing inclusions and slower in the inclusions with coarser-grained mesostases.

As the cooling rates of the inclusions were not all the same at high-temperatures (≥1000°C), the cooling environments of different inclusions were not precisely the same at high temperatures. Thus, if the inclusions are co-genetic, they may have cooled in an environment that had a substantial temperature gradient, consistent with a near-surface setting within the parent body.

Rapid solidification of inclusions is also implied by the large density contrast between the inclusions and the dense metallic host, together with textural evidence that the FeNi-metal host may have been molten or semi-molten (Takeda et al., 1998). If the metallic host were substantially molten, as suggested by the physical projection of silicate phases into the surrounding FeNi-metal host (see above; and Takeda et al., 1998), the silicates could not have remained entrained within the metal for long periods of time in the presence of even a weak gravitational field, unless turbulence in the metallic melt kept the inclusions from rising buoyantly.

In principle, homogenization during metamorphism could explain the uniform major-element compositions of plagioclase, and the tendency for trace-element abundances in the same phases from different inclusions to be similar, but metamorphic homogenization is unlikely to have been important. Major-element interdiffusion rates in plagioclase are slower than in clinopyroxene (Brady and McCallister, 1983; Grove et al., 1984), implying that plagioclase would have become closed to diffusion at temperatures even higher than that of augite (~1000–1100°C), within the range expected for igneous pro-

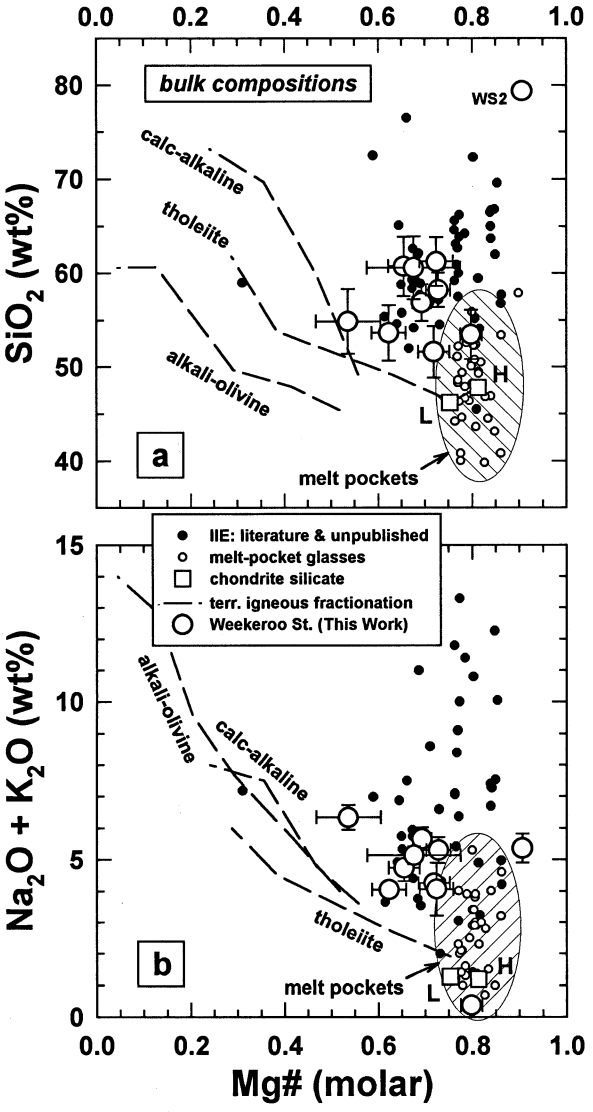

Fig. 8. Mg# (= Mg/[Mg + Fe^{2+}]) vs. SiO_2 (a) and alkali (b) abundances in silicate inclusions from Weekeroo Station (This Work, Table 4), and other IIE and IIE-related meteorites (Appendix 1), compared to terrestrial volcanic fractionation trends (McBirney, 1992), melt-pocket glasses (shaded areas) in L-group chondrites (Dodd and Jarosewich, 1982; Dodd et al., 1982), and average H-group and L-group ordinary chondrite silicate (Jarosewich, 1990). The chemical trends shown by IIE silicate inclusions are unlike the differentiation trend shown by terrestrial volcanic rocks.

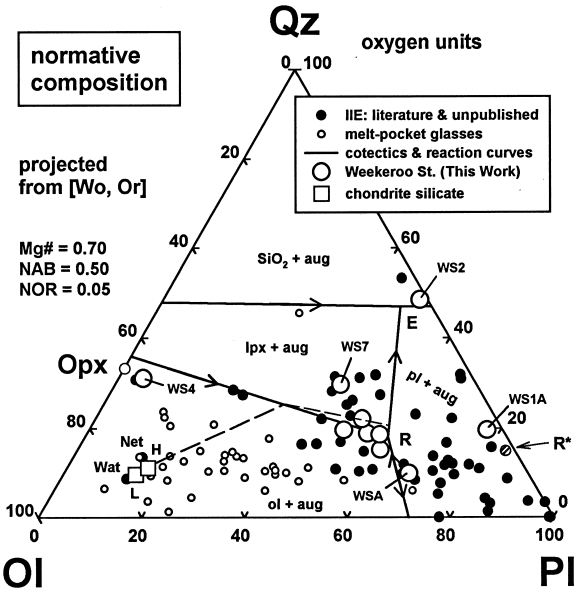

Fig. 9. Normative compositions of IIE silicate inclusions projected from wollastonite (Wo) and orthoclase (Or) onto the augite-saturated Olivine (Ol)-Quartz (Qz)-Plagioclase (Pl) ternary liquidus diagram of Longhi (1991), for equilibria corresponding to Mg# = 0.70, normative albite (NAB) = 0.50, and normative orthoclase (NOR) = 0.05. E represents the eutectic composition; R represents the olivine-pyroxene-feldspar reaction point. With increasing NAB, points E and R shift to the right. R* is the composition of the peritectic in the forsterite-quartz-nepheline system (Schairer and Yoder, 1961) and is appropriate to a system with Mg# = 1 and NAB = 1. A fractional crystallization liquid path originating from H-chondrite silicate is shown schematically by the dashed line; solid lines with arrows represent cotectics or reaction curves. Data sources as in Fig. 8. Molar abundances of oxides were converted to normative abundances using the following algorithm: Pl = 8(Al_2O_3 − K_2O + Na_2O), Wo = 3(CaO − Al_2O_3 + K_2O + Na_2O), Ol = 2(MgO + FeO + MnO), Qz = 2SiO_2 − 10 Na_2O − 10 K_2O − 2 CaO − 2 Al_2O_3 − MgO − FeO − MnO. See Text.

cesses. Rates of REE diffusion in plagioclase and pyroxene are not known, but they are unlikely to have been faster than for major-element interdiffusion, as a result of the charge-coupled substitutions necessary. This implies that the REE abundances of plagioclase and augite (and possibly orthopyroxene) in the inclusions were unaffected by metamorphism.

7.2. Differentiation and Parental Melts

Estimates were made of the REE abundances of parental melts in equilibrium with augite, orthopyroxene, and plagioclase, using the mineral-melt partition coefficients (D-values) given in Table 6. The D-values for augite correspond to a clinopyroxene with the appropriate Wo content (~Wo_{37}), but the value for D_{Eu} may be underestimated, as it corresponds to the partitioning of Eu in a relatively oxidized melt (a shergottitic melt including a rather high Fe^{3+}/Fe^{2+} ratio), and not the relatively reduced melt appropriate for IIE iron meteorites. For plagioclase, the D-values estimated by Papike et al. (1997) were assumed, although they depend greatly on temperature and composition (Drake and Weill, 1975). For orthopyroxene, the median D-values of Schwandt and McKay (1996) were used, which are appropriate for diogenite-like orthopyroxene.

The calculated parental melt compositions are shown in Fig. 13a. The parent melts for augite and plagioclase have relatively flat REE patterns, with abundances of ~20–30 × CI-chondrites for most REE, except for a negative Eu anomaly (Fig. 13a). In contrast, the calculated melt for orthopyroxene has much lower abundances of HREE, and appears to show a positive Eu anomaly (Fig. 13a). The latter is, however, uncertain owing to the low abundances of Eu in the orthopyroxene. The overall agreement between the calculated parental melts for augite and plagioclase implies that they could have crystallized from the same melt. The different results for orthopyroxene may indicate that it crystallized from a different melt, that

Table 5a. Trace-element abundances in pyroxenes.

WS incl.	*1B aug*	*1B opx*	*1B opx*	*7 aug*	*7 aug*	*7 aug*	*4 opx*	*4 opx*	*avg. aug*	*avg. opx*
anal. #	P1	P2	P3	P1	P2	P3	P1	P2		
μg/g[‡]									CI-normalized[†]	
Sr	5.81	0.06	1.02	10.0	6.81	5.32	0.22	0.11	0.90	0.05
Y	12.7	0.57	1.01	11.1	11.2	10.8	0.56	0.30	7.32	0.39
Zr	33.1	1.42	6.71	7.28	3.71	3.36	0.18	0.12	3.01	0.53
La	0.28	—	0.03	0.23	0.14	0.14	0.01	—	0.84	0.04
Ce	1.54	0.01	0.16	1.42	0.68	0.61	0.05	0.01	1.76	0.10
Nd	2.01	(0.01)	0.07	2.01	1.18	1.07	0.03	0.02	3.46	0.07
Sm	1.22	0.04	0.02	1.06	1.00	0.80	0.04	0.04	6.93	0.24
Eu	0.07	(0.02)	(0.01)	0.11	0.10	0.04	(0.01)	—	1.42	0.24
Dy	2.01	0.10	0.12	1.89	1.79	1.50	0.10	0.04	7.41	0.37
Er	1.23	0.06	0.08	1.02	1.03	0.80	0.05	0.05	6.42	0.38
Yb	1.58	0.13	0.18	0.94	0.81	0.83	0.09	0.05	6.40	0.69

[†] CI-chondrite abundances of Anders and Grevesse (1989) used for normalization.
[‡] Values in parentheses are close to estimated background levels and are considered uncertain.

Table 5b. Trace-element abundances in plagioclase.

WS incl.	*1B*	*1A*	*1A*	*1A*	*avg. plagioclase*
anal. #	F1	F2	F3	F4	
μg/g[‡]					CI-normalized[†]
Sr	117	127	136	117	15.9
Y	0.02	0.19	0.08	0.10	0.06
Ba	44.6	52.9	51.6	46.6	20.9
La	0.23	0.86	0.80	0.66	2.72
Ce	0.46	1.67	1.77	1.13	2.09
Nd	0.08	0.55	0.56	0.31	0.83
Sm	—	0.04	0.15	0.09	0.64
Eu	0.81	1.25	1.11	1.00	18.5
Dy	(0.02)	(0.20)	0.09	0.04	0.26
Er	(0.03)	(0.11)	0.04	(0.04)	—
Yb	—	(0.10)	0.03	—	—

[†] CI-chondrite abundances of Anders and Grevesse (1989) used for normalization.
[‡] Values in parentheses may reflect the effects of beam overlap with surrounding phases and were excluded from the average.

Table 5c. Trace-element abundances in glass.

WS incl.	*2*	*2*	*2*	*7*	*7*	*avg.*	*opx + plag*
anal. #	G1	G2	G3	G1	G2	*glass*	*mixture*[§]
μg/g						CI-normalized[†]	
Sr	10.8	38.6	31.0	31.1	33.0	3.70	3.70
Y	0.17	0.18	0.19	0.58	1.30	0.31	0.32
Zr	8.71	8.53	8.67	31.1	35.9	4.71	—
La	0.03	0.02	0.02	0.15	0.34	0.48	0.66
Ce	0.08	0.07	0.05	0.29	0.56	0.35	0.55
Nd	0.02	0.05	0.11	0.17	0.48	0.37	0.25
Sm	0.01	0.01	0.02	0.02	0.06	0.16	0.33
Eu	0.05	0.42	0.36	0.37	0.36	5.58	4.45
Dy	0.06	0.02	0.02	0.09	0.24	0.35	0.35
Er	0.04	0.09	0.06	0.13	0.16	0.60	—
Yb	0.01	0.03	0.02	0.07	0.08	0.26	—

[†] CI-chondrite abundances of Anders and Grevesse (1989) used for normalization.
[§] 77 wt% avg. opx (Table 5a) + 23% avg. plag (Table 5b).

the D-values for orthopyroxene are inappropriate, or that the trace-element composition for orthopyroxene grains reflect a disequilibrium process. In the discussion that follows, we focus on the data for augite and plagioclase and model how parental melts of the appropriate composition for these phases may have formed.

Although the data for augite and plagioclase suggest the presence of a negative Eu anomaly in the parental melt, the size

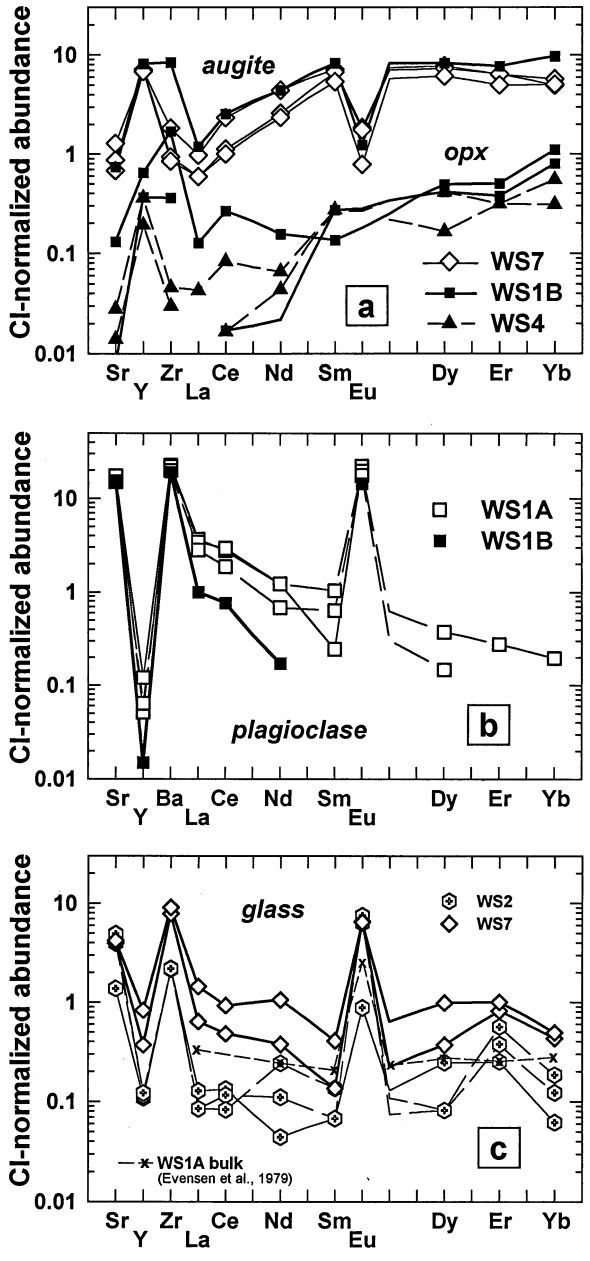

Fig. 10. CI-normalized abundances of trace-elements in (a) orthopyroxene and augite, (b) plagioclase, and (c) glass in Weekeroo Station inclusions. Data are from Table 5. The CI abundances of Anders and Grevesse (1989) were used for normalization.

of the inferred anomaly is not exactly the same for each phase. This may be caused by an inappropriate choice of D_{Eu} for augite, as noted above. Lowering D_{Eu} for augite, as seems more appropriate for reducing conditions, will result in an increase in the inferred Eu concentration of the parental melt for augite, bringing the calculated Eu value for this melt into closer agreement with that calculated for plagioclase.

In general, the relatively unfractionated or perhaps LREE-enriched pattern of the calculated melts for augite and plagioclase is consistent with the partial melting of a chondritic source. The negative Eu anomaly implies incomplete melting

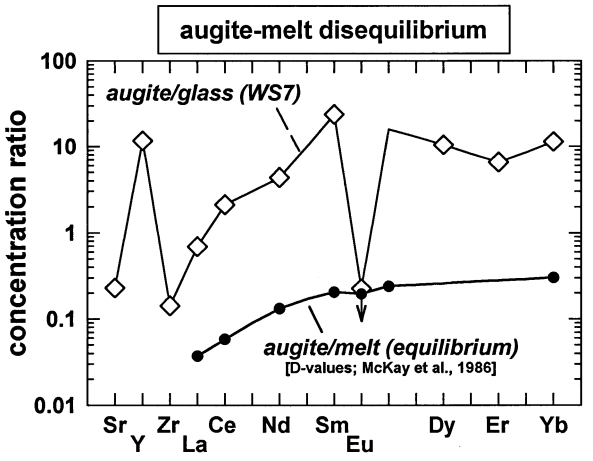

Fig. 11. Evidence for significant augite-melt disequilibrium for the REEs in inclusion WS7 is provided by the large discrepancy between the augite/glass concentration ratio (data from Table 5a, c) and experimentally-determined mineral/melt partition coefficients (Mckay et al., 1986; Table 6). See Text.

of plagioclase in the source region, or the segregation of plagioclase by fractional crystallization. For equilibrium partial melting of an H-group-chondrite precursor, plagioclase is exhausted for $\geq$15% partial melting (Taylor et al., 1993). Thus, if the inclusions were produced by single-stage partial melting of a chondritic source, a low degree of partial melting ($<$15%) would be necessary to produce the inferred parental melts for plagioclase and augite.

More quantitative constraints on the differentiation process can be obtained by modelling the REE abundances of partial

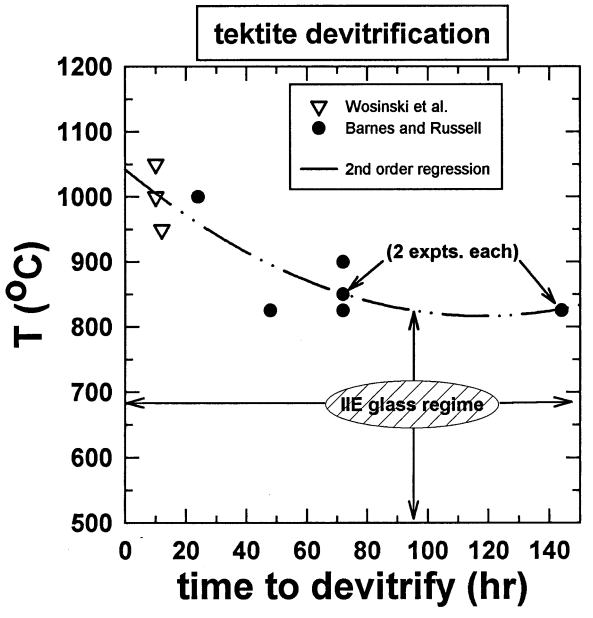

Fig. 12. Plot summarizing the results of devitrification experiments on tektite compositions (Barnes and Russell, 1966; Wosinski et al., 1967), and the inferred time-temperature regime for glass-rich IIE inclusions to prevent significant devitrification of the glass. See Text.

Table 6. Mineral/melt partition coefficients used in this study.

	Plagioclase[1]	Augite[2]	Orthopyroxene[3]	Olivine[4]
La	0.036	0.036	0.0006	0.0001
Ce	0.031	0.057	0.0011	0.0001
Nd	0.026	0.132	0.0040	0.0001
Sm	0.02	0.205	0.0115	0.0006
Eu	1.15	0.195	0.0048	0.0007
Gd	0.016	0.236	0.0292	0.001
Dy	0.013	0.258	0.0469	0.003
Er	0.010	0.280	0.0733	0.008
Yb	0.007	0.302	0.1288	0.019

[1] Calcic plagioclase; Papike et al. (1997), after Jones (1995) and Phinney and Morrison (1990).
[2] Wo_{37} augite; McKay et al. (1986).
[3] Diogenite-like orthopyroxene; average of "high" and "low" values from Schwandt and McKay (1996).
[4] McKay (1986).

melts in chondritic systems. We used the average composition of the silicate portion of H-group chondrite falls (Jarosewich, 1990) as the assumed starting composition of the protolith, and assumed both one-stage and two-stage differentiation models. For one-stage differentiation, we modelled equilibrium modal batch melting, equilibrium non-modal batch melting, and fractional melting. The proportion of phases being melted in non-modal melting was estimated from the peritectic composition of an H-group melt using the appropriate ternary diagrams of Longhi (1991). For the two-stage differentiation model, it was assumed that non-modal batch melting (≤20%) was followed by fractional crystallization of orthopyroxene, augite, and plagioclase in approximate cotectic proportions.

The calculated melt compositions for one-stage models involving 2–5% modal batch melting and 0.5% fractional melting are shown in Fig. 13b. These conditions produce melts broadly similar in composition to that implied by the data for augite and plagioclase. The results for non-modal batch melting generally are similar to that of modal batch melting, except that slightly more LREE-enriched melts are produced. All of these cases result in a negative Eu anomaly of roughly the appropriate magnitude, and abundances of Sm, Dy, Er, and Yb that are in agreement with the data. The results suggest that a very low degree of partial melting (≤5%) of an H-chondrite precursor could have produced the parental melts out of which augite and plagioclase crystallized.

Fig. 13c shows the compositions of melts produced in a two-stage model involving higher degrees of partial melting (10–20%) followed by 55–75% cotectic fractional crystallization of pyroxene and plagioclase. The calculated melt compositions for these conditions are in substantial agreement with the data. Thus, higher degrees of partial melting (10–20%) of an H-chondrite precursor, coupled with fractional crystallization of these melts, could have also produced the parental melts out of which augite and plagioclase crystallized.

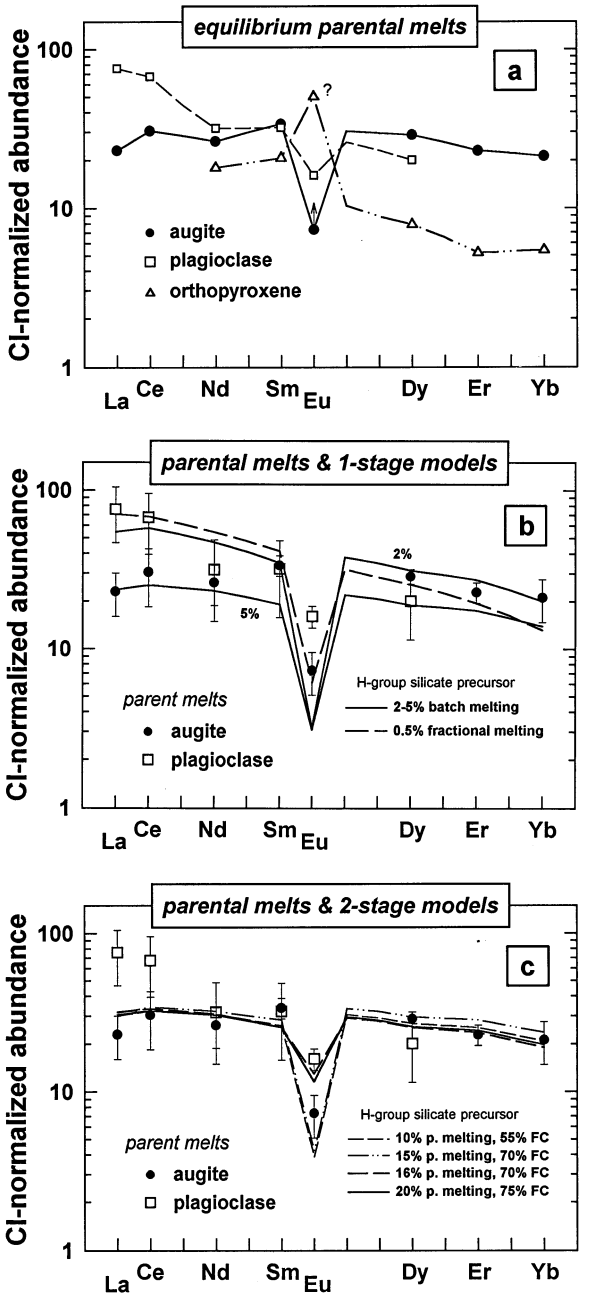

Fig. 13. CI-normalized abundances for calculated parental melts in equilibrium with augite, plagioclase, and orthopyroxene (a), compared to 1-stage (b) and 2-stage (c) differentiation models. Calculations assume an average composition of augite, orthopyroxene, and plagioclase (Table 5a–b), the partition coefficients given in Table 6, and (for the differentiation models) an H-group silicate precursor. Data points are shown for the parental melts only in cases that have multiple determinations for a given element in a given phase, and that have standard deviations of average compositions less than 100%. Error bars in (b) and (c) reflect the uncertainties of the average mineral compositions (±1 standard deviation), and do not take into account any uncertainties in partition coefficients. See Text.

7.3. Impact-induced Differentiation?

Notwithstanding the simple differentiation models that can explain the rare-earth-element data for augite and plagioclase, it was noted that the bulk major-element compositions of silicate inclusions in IIE meteorites scatter widely and are inconsistent with terrestrial-style differentiation trends (Fig. 8, 9). Rubin et al. (1986) suggested that silicate inclusions in IIE meteorites formed by shock-melting, based on the chemical

similarity between a large silicate inclusion in the Guin silicated iron meteorite and that of melt-pocket glasses in ordinary chondrites, which clearly formed by localized, shock-induced melting (Dodd and Jarosewich, 1979, 1982; Dodd et al., 1982; Stoffler et al., 1988, 1991). Gaffey and Gilbert (1998) suggested that IIE irons formed in impact-produced melt pools on the H-chondrite parent body, possibly the asteroid 6 Hebe. That hypervelocity impact processes were important for IIE inclusions is suggested by relatively young ages for some of them (Snyder et al., 1999), and by the inference that they cooled in a near-surface environment on their parent body (see above). However, the question remains whether impact processes were responsible for the differentiation of IIE silicate inclusions.

This can be evaluated by comparing the bulk, major-element compositions of IIE inclusions and that of melt-pocket glasses in ordinary chondrites (Fig. 8, 9). The IIE inclusions are similar to melt-pocket glasses in having relatively uniform Mg# (Fig. 8) and in being enriched in a plagioclase component relative H and L-chondrite silicates (Fig. 9). Both melt-pocket glasses in chondrites (Dodd and Jarosewich, 1982; Dodd et al., 1982) and agglutinate glasses in lunar soils (e.g., Papike et al., 1982; Walker and Papike, 1981) are enriched in a feldspar component, as a result of preferential melting of feldspar during shock processes. Experimental evidence for preferential shock-melting of feldspar is also observed in basaltic targets (Schaal and Horz, 1977; Schaal et al., 1979). Conceivably, a similar feldspar-enrichment process could explain the feldspathic compositions of most IIE inclusions.

However, the compositions of IIE silicate inclusions scatter more widely than that of melt-pocket glasses, and they are more enriched in a feldspar component than the glasses (Fig. 9). Moreover, no IIE inclusion analyzed to date has a composition that lies within the main melt-pocket field (Fig. 9). A large compositional hiatus occurs between the "primitive" inclusions found in Watson and Netschaëvo and the "fractionated" inclusions found in meteorites such as Weekeroo Station, and it is in this hiatus that most melt-pocket glasses fall (Fig. 9). These differences imply that IIE silicate inclusions did *not* form in precisely the same way as melt-pocket glasses. Moreover, some have argued that shock-melting can produce only small volumes of fractionated melt (Keil et al., 1997), smaller than required for IIE inclusions. Thus, the evidence for shock-induced differentiation of IIE inclusions is equivocal. More studies on chemically fractionated impact-melts are needed to resolve this issue.

7.4. Remelting

Evidence for a remelting process is provided by the distinctive trace-element compositions of silica-rich glasses in some inclusions. As noted above, the trace-element compositions of these glasses are unlike those expected for evolved igneous melts, and the glass in one inclusion does not appear to be in equilibrium with co-existing pyroxene in the inclusion.

Fig. 14 and Table 5c show that a mixture of 23 wt% average plagioclase and 77% average orthopyroxene provides a good match to the average trace-element composition of the glass for all elements. The match is especially good for Sr, Y, Eu, and Dy (Fig. 14), elements which have significantly different mineral-melt partition coefficients in plagioclase and orthopyroxene (e.g., Table 6), and which have significantly different abundances in the analyzed plagioclase and orthopyroxene grains (Fig. 10a–b; Table 5a–b). For example, Sr and Eu are strongly enriched in plagioclase compared to orthopyroxene, whereas Y is enriched in orthopyroxene compared to plagioclase (Fig. 10a–b). The fact that a hypothetical mixture of plagioclase and orthopyroxene can yield a good match to the average abundance of these elements in the glass is unlikely to be coincidental, and strongly suggests that the glass formed by the remelting of pre-existing plagioclase and orthopyroxene.

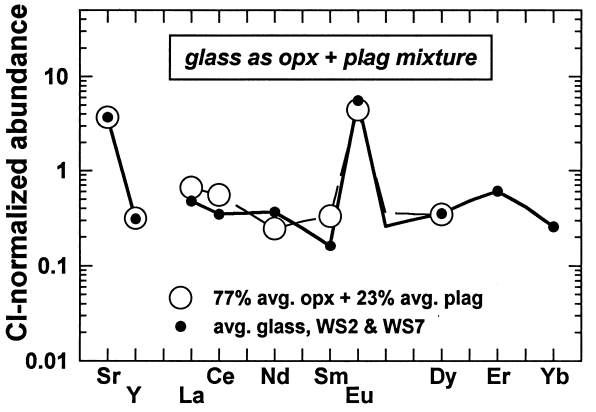

Fig. 14. The CI-normalized abundances of a variety of trace elements in average Si-rich glass are compared to a hypothetical mixture of 77 wt% average orthopyroxene and 23% average plagioclase (Table 5c), showing a good match for all elements in which the comparison can be made. The match implies that the glass could have formed by the re-melting of pre-existing orthopyroxene and plagioclase. In contrast, models involving augite as a component in a hypothetical mixture could not be made to fit with the glass data. The CI abundances of Anders and Grevesse (1989) were used for normalization.

It seems unlikely that the melt which produced the glass was produced by equilibrium partial melting of plagioclase and orthopyroxene. One reason is that the calculated equilibrium parental melts for these phases are different (Fig. 13a). Another is that the low abundances of REE in the glass (Fig. 10c) are unlike what one would expect of an equilibrium partial melting process involving plagioclase and orthopyroxene. Instead, it appears that the glass was derived from a plagioclase and orthopyroxene mixture either by disequilibrium melting, or by the substantial (and possibly total) melting of these phases.

To melt only these two minerals and not several others suggests that a noritic target may have been melted. Alternatively, selective melting of essentially only these two phases, perhaps caused by hypervelocity impact, can also explain the data. With regard to the latter possibility, an intriguing similarity exists between the proportion of orthopyroxene and plagioclase inferred for the melt based on trace-element data (orthopyroxene:plagioclase in the mixture to produce glass = 77:23) and that found in ordinary chondrites (normative orthopyroxene:plagioclase in H-chondrites = 73:27). This similarity could indicate that the melt that produced the glass was derived by nearly total melting of pre-existing orthopyroxene and plagioclase from an ordinary chondrite protolith.

Although evidence for remelting is strongest for those inclusions that contain glass, there are indications that other inclusions also were remelted. For example, the bulk major- and

trace-element composition of crystalline felsic inclusion WS1A is very similar to the glass in WS2 and WS7 (Fig. 7, 10c). This implies that inclusion 1A is simply a crystallized variant of the glass, and that it otherwise formed in the same way. Similarly, the textural evidence for relict pyroxene grains in inclusions 4, 10A, and 5A is consistent with two episodes of melting: an earlier episode that crystallized the coarse, possibly relict pyroxenes, and a later episode that crystallized the remainder of the inclusions. Finally, remelting is also consistent with evidence for two chemical trends in orthopyroxene (Trend 1 and 2, Fig. 5), which may reflect two episodes of crystallization under different redox conditions.

7.5. Reduction

Data for orthopyroxene and glass imply that the inclusions experienced reduction of FeO, after metal-silicate mixing, and during the remelting event that appears to have affected the inclusions. As noted above, the composition of Trend 2 orthopyroxene grains (Fig. 5) appears to reflect both igneous fractionation and FeO-reduction by reaction with the FeNi-metal host. These orthopyroxene grains crystallized from, or equilibrated with, a silicate melt that was undergoing FeO-reduction. The relevant redox reaction could have been similar to the reaction proposed by Ikeda et al. (1997a) for inclusions in Miles:

$$\underset{Melt}{5FeO} + \underset{Melt}{3CaO} + \underset{Metal}{2P^{o}} \rightarrow \underset{Metal}{5Fe^{o}} + \underset{Phosphate}{Ca_3(PO_4)_2}. \quad (1)$$

Any orthopyroxene crystallizing from a melt undergoing this reaction would tend to have low Fs and Wo contents, as observed for Trend 2 orthopyroxenes close to the FeNi-metal host. This reaction can also explain the tendency for phosphate to occur near the interfaces between silicate inclusions and the metal host.

Evidence for FeO-reduction is also provided by the silica-rich glasses, albeit in a more indirect manner. As noted above, trace-element data imply that such glasses were produced by the remelting of pre-existing plagioclase and orthopyroxene. However, the glasses contain very little (<5 mol%) normative orthopyroxene (Table 3c), and instead consist almost exclusively of normative plagioclase and *quartz* (Fig. 7). Evidently, substantial amounts of normative orthopyroxene must have been transformed to normative quartz during remelting. This requires the loss of FeO and MgO originally present in orthopyroxene to other phases. The FeO could have been reduced to Fe-metal by reaction [1], with this metal becoming incorporated in the surrounding host. The MgO could have been incorporated into a second generation of pyroxene, such as is now represented by Trend 2 orthopyroxene. The reaction for the remelting of orthopyroxene may be expressed as follows:

$$\underset{Remelted\ opx}{MgSiO_3} + \underset{Metal}{FeSiO_3} \rightarrow \underset{Melt}{Fe^{o}} + \underset{Secondary\ opx}{SiO_2 + MgSiO_3} + 0.5O_2. \quad (2)$$

Reactions [1] and [2] could be different aspects of the same overall process. Reaction [1] emphasizes the change in melt composition and the crystallization of phosphate, whereas reaction [2] emphasizes the inferred breakdown of orthopyroxene to silica-rich melt, Fe-metal, and a second generation of Mg-orthopyroxene by remelting and reduction.

Reactions [1] and [2] may have operated together to form the Mg-rich orthopyroxene coronas that surround large augite grains (relict grains?) elsewhere in WS (Bunch et al., 1970) and other IIE irons (Rubin et al., 1986; Ikeda and Prinz, 1996; Ikeda et al., 1997a; Takeda et al., 1998). To produce the coronas, the enstatite component of the augite could be used to make corona Mg-orthopyroxene by reaction [2], "and the wollastonite component could be used to make phosphate by reaction [1]."

Unlike orthopyroxene, augite does not show chemical variations that can be attributed to redox processes. Possibly, faster major-element interdiffusion rates in orthopyroxene compared to clinopyroxene (Brady and McCallister, 1983; Ganguly and Tazzoli, 1994) led to more rapid response of orthopyroxene to changing equilibration conditions. Alternatively, differences in susceptibility to melting in a rapid reheating process (i.e., preferential melting of orthopyroxene?), or in the timing of crystallization relative to reduction, could have been important in establishing redox-related chemical variations in orthopyroxene but not augite.

Extensive FeO-reduction of melts may explain, in part, why bulk inclusion compositions scatter (Fig. 9) and why Mg# is not correlated with silica or alkali abundances (Fig. 8) (Ikeda and Prinz, 1996; Ikeda et al., 1997a). Conceivably, an extreme degree of FeO-reduction could also explain the dearth of olivine in IIE inclusions of the fractionated type, by the breakdown of olivine to orthopyroxene and the conversion of FeO to Fe-metal. However, FeO-reduction alone cannot account for the diverse compositions of IIE inclusions.

7.6. Dynamic Mixing

A variety of observations suggest that a physical mixing process played an important role in the formation of the silicate inclusions. Evidence for "dynamic mixing" includes the following.

1. The large variations of modes and bulk compositions, but the similar major- and trace-element compositions for the same phases in different inclusions, is best explained by sampling different proportions of the same phases that were derived from common precursors. As noted above, the relatively uniform compositions of phases from different inclusions are probably not the result of homogenization during thermal metamorphism, leaving derivation of phases from common precursors as the most likely explanation. To produce bulk-chemical diversity, "mixing" could have involved either a dynamic process involving movement of material, or non-representative sampling during the remelting of a coarse-grained precursor (Prinz et al., 1983).
2. The presence of a pyroxene-glass inclusion that exhibits evidence for large disequilibrium between the co-existing augite grains and glass (Fig. 11) can be explained if the augite did not crystallize in a closed system from the same melt now represented by the glass. In other words, the glass and augite may have been derived from different source materials that were later mixed together, probably during the

remelting event that appears to have produced the glass (see above).
3. The preferential alignment of pyroxene grains in some inclusions is consistent with their formation in a stress or flow field, consistent with a dynamic mixing process.
4. The existence of coarse, and sometimes highly irregular, pyroxene grains in otherwise fine-grained inclusions is consistent with a process involving physical transport of material, and with the mechanical disruption of the coarse pyroxene grains.

Dynamic mixing of silicate phases appears to have occurred no later than the remelting process inferred for the inclusions, and, considering the evidence for FeO-reduction by reaction with the FeNi-metal host during remelting (see above), no later than the metal-silicate mixing event that formed the IIE irons. Most likely, dynamic mixing of the silicates occurred at the same time as metal-silicate mixing. Such mixing was probably shock-induced.

8. MODELS FOR FORMING IIE IRON METEORITES

A synthesis of this study with previous work suggests two possible models for forming IIE iron meteorites, both involving collision between an FeNi-metal impactor (probably the core of a differentiated planetesimal stripped of its overlying silicate) and a silicate-rich target of H-chondrite affinity. A metal impactor is the logical source of the large amount of native metal present in the meteorites, whereas the silicate-rich target is the source of the silicate inclusions. Recent support for one or more collisions between different parent bodies to form IIE meteorites comes from Hf-W isotopic studies of Watson (Snyder et al., 1999) and Re-Os isotopic studies of Kodaïkanal (Birck and Allègre, 1998).

In the first model, the collision occurs between the metal impactor and an already-differentiated target, and the metal impactor remelts and mixes with the Si-rich crust of the target to produce IIEs with fractionated silicates. In this model, IIE iron meteorites could have been produced in a process analogous to that which formed mesosiderites, except that remelting may have been more pronounced for the IIEs.

There are two significant attributes to this model. First, it can readily account for the presence of coarse-grained material (orthopyroxene and clinopyroxene) in IIE silicate inclusions, some of which may have been derived from pre-existing, coarse-grained precursors, by the operation of crust-forming processes in a slowly-cooling environment. Second, it explains the dearth of olivine in IIE iron meteorites that have fractionated inclusion types, by the sequestering of olivine in the mantle of the differentiated target (Prinz et al., 1982). To avoid oversampling olivine, the postulated impact event could not have mixed materials from the mantle of the target.

The main drawback of this model is that it cannot also easily explain the occurrence of IIE meteorites with unfractionated silicates, such as Watson, Netschaëvo, Techado, and the possibly related, but unclassified meteorite, Yamato-791093 (Ikeda et al., 1997b). In particular, the presence of relict chondrules in all of these meteorites, except for Watson, suggests that the silicates were not totally melted, inconsistent with a wholly-differentiated target. Either the target was only locally differentiated, or H-chondrite-like material was added to the differentiated target at some later stage.

In the second model, a collision occurs between the FeNi-metal impactor and an undifferentiated target (Wasson and Wang, 1986). Depending on their original position in the target asteroid relative to the impact site, silicates remain either unmelted (Techado, Netschaëvo), or melted but undifferentiated (Watson), or extensively differentiated (other IIE irons). Differentiation occurs by impact-melting during the collision. Metal and silicate mix either on the surface of the parent body in an impact-melt pool, or in an ejecta blanket that is later remelted. A variant of this model is that the impactor contributes little material to the final metal-silicate mixture, and metal is derived instead from the undifferentiated target (Ikeda et al., 1997b; Ebihara et al., 1997). In this type of model, metal is presumably concentrated by impact-melting.

Collision with an undifferentiated target can better account for the existence of IIE irons with unfractionated silicates. This model is preferred for Watson, as W-isotope data for a large silicate inclusion in this meteorite imply that the silicate was derived from a source region, such as a chondritic parent body, that did not experience early Fe-Ni-core formation (Snyder et al., 1999). However, collision with an undifferentiated parent body has more difficulty in accounting for the IIE irons with fractionated silicates, as it requires extensive differentiation to occur by impact-melting, which is unproven and possibly unlikely (Keil et al., 1997), and it has difficulty in accounting for the near-absence of an olivine component in either the melt pool or in the ejecta blanket produced during the collision. Collision with an undifferentiated parent body also has difficulty in accounting for the presence of coarse-grained pyroxene in fractionated IIE silicate assemblages, as an impact-melt would probably cool too rapidly to produce such coarse-grained phases.

Thus, it appears that collision of an FeNi-metal body with a differentiated silicate body can better account for IIE irons such as Weekeroo Station, which contain evolved silicates, and that collision with an undifferentiated silicate body can better account for IIE irons with unfractionated or incompletely-melted chondritic inclusions, such as Techado, Netschaëvo, and Watson. Although perhaps philosophically dissatisfying, each of these models may be correct for different IIE iron meteorites. This would be consistent with the apparent dichotomy of IIE irons into one group that contains fractionated inclusions only, and into another group that contains unfractionated inclusions only. Possibly, similar collisional processes occurred on two different H-chondrite-like target bodies, one that was differentiated, and one that was not, yielding the diverse IIE group. Iron meteorites such as Sombrerete and Guin could have formed by the collision of similar FeNi-metal impactors with yet different types of target asteroids.

9. CONCLUSIONS

Silicate inclusions in the Weekeroo Station IIE iron meteorite were studied using petrographic, EMP, and SIMS techniques. The petrogenesis of these inclusions appears to have been complex, and involved differentiation, remelting, FeO-reduction, and dynamic mixing of phases. Differentiation produced a variety of olivine-free inclusion assemblages from a

presumed H-chondrite protolith, modelled as having involved either low degrees of partial melting (2–5%), or higher degrees of partial melting (e.g., 10–20%) coupled with subsequent fractional crystallization. At least some, and perhaps all, inclusions were remelted, producing glass that formed by the remelting of pre-existing plagioclase and orthopyroxene. Remelting was accompanied by reduction of FeO in the melts by reaction with the enclosing FeNi-metal host. Differences in inclusion mineralogies, modes, and textures probably arose, in part, by mechanical separation of pre-existing phases, in an impact event that dynamically mixed silicates with the metallic host. Following melting, the inclusions cooled relatively rapidly at different rates, most likely in a near-surface setting in the parent body. The results of this study suggest that IIE iron meteorites could have formed by the collision between an FeNi-metal impactor and either a differentiated or undifferentiated silicate-rich target of H-chondrite affinity. More than one type of target may be necessary to account for the full diversity of IIE-like meteorites.

Acknowledgments—This work was supported by NASA grants NAGW 3543 (LAT) and NAGS-4745 (MP). The authors wish to dedicate this paper to Grant Fowler, whose untimely death is of deep regret. His presence will be missed.

REFERENCES

Anders E. and Grevesse N. (1989) Abundances of the elements: Meteoritic and solar. *Geochim. Cosmochim. Acta* **53,** 197–214.

Armstrong J. T., Kennedy A. K., Carpenter P. K., and Albee A. L. (1990) Petrography and trace element chemistry of Colomera (IIE) silicate inclusions; rhyolitic plums in the pudding. *Lunar Planet. Sci.* **XXI,** 22–23.

Barnes V. E. and Russell R. V. (1966) Devitrification of glass around collapsed bubbles in tektites. *Geochim. Cosmochim. Acta* **30,** 143–152.

Bence A. E. and Burnett D. S. (1969) Chemistry and mineralogy of the silicates and metal of the Kodaikanal meteorite. *Geochim. Cosmochim. Acta* **33,** 387–407.

Birck J. L. and Allègre C. J. (1998) Rhenium-187 and Osmium-187 in iron meteorites and the strange origin of the Kodaïkanal meteorite. *Meteorit. Planet. Sci.* **33,** 647–653.

Brady J. B. and McCallister R. H. (1983) Diffusion data for clinopyroxenes from homogenization and self-diffusion experiments. *Amer. Mineral.* **68,** 95–105.

Buchwald V. F. (1975) *Handbook of iron meteorites—Their history, distribution, and composition and structure*. Vol. 1–3. University of California Press.

Bunch T. E. and Olsen E. (1968) Potassium feldspar in Weekeroo Station, Kodaikanal, and Colomera Iron Meteorites. *Science* **160,** 1223–1225.

Bunch T. E., Keil K. and Olsen E. (1970) Mineralogy and petrology of silicate inclusions in iron meteorites. *Contrib. Mineral. Petrol.* **25,** 297–340.

Casanova I., Graf T. and Marti K. (1995) Discovery of an unmelted H-chondrite inclusion in an iron meteorite. *Science* **268,** 540–542.

Clayton R. N. and Mayeda T. K. (1996) Oxygen isotope studies of achondrites. *Geochim. Cosmochim. Acta* **60,** 1999–2017.

Clayton R. N., Mayeda T. K., Olsen E. J., and Prinz M. (1983) Oxygen isotope relationships in iron meteorites. *Earth Planet. Sci. Lett.* **65,** 229–232.

Dodd R. T., and Jarosewich E. (1979) Incipient melting in and classification of L-group chondrites. *Earth Planet. Sci. Lett.* **44,** 335–340.

Dodd R. T., and Jarosewich E. (1982) The compositions of incipient shock melts in L6 chondrites. *Earth Planet. Sci. Lett.* **59,** 355–363.

Dodd R. T., Jarosewich E., and Hill B. (1982) Petrogenesis of complex veins in the Chantonnay (L6f) chondrite. *Earth Planet. Sci. Lett.* **59,** 364–374.

Ebihara M., Ikeda Y., and Prinz M. (1997) Petrology and chemistry of the Miles IIE iron. II. Chemical characteristics of the Miles silicate inclusions. *Antarct. Meteorites Res.* **10,** 373–388.

Evensen N. M., Hamilton P. J., Harlow G. E., Klimentidis R., O'Nions R. K. and Prinz M. (1979) Silicate inclusions in Weekeroo Station: Planetary differentiates. *Lunar Planet. Sci.* **X,** 376–377.

Gaffey M. J. and Gilbert S. L. (1998) Asteroid 6 Hebe: The probable parent body of the H-type ordinary chondrites and the IIE iron meteorites. *Meteorit. Planet. Sci.* **33,** 1281–1295.

Ganguly J. and Tazzoli V. (1994) Fe^{2+}-Mg interdiffusion in orthopyroxene: Retrieval from the data on intracrystalline exchange reaction. *Amer. Mineral.* **79,** 930–937.

Grove T. L., Baker M. B. and Kinzler R. J. (1984) Coupled CaAl-NaSi diffusion in plagioclase feldspar: Experiments and application to cooling rate speedometry. *Geochim. Cosmochim. Acta* **48,** 2113–2121.

Hsu W., Takeda H., Huss G. R., and Wasserburg G. J. (1977) Mineralogy and chemical compositions of Colomera (IIE) silicate inclusions. *Meteorit. Planet. Sci.* **32,** A61–A62 (abstract).

Ikeda Y. and Prinz M. (1996) Petrology of silicate inclusions in the Miles IIE iron. *Proc. NIPR Symp. Antarct. Meteorites* **9,** 143–173.

Ikeda Y., Ebihara M. and Prinz M. (1997a) Petrology and chemistry of the Miles IIE iron. I. Description and petrology of twenty new silicate inclusions. *Antarct. Meteorite Res.* **10,** 355–372.

Ikeda Y., Yamamoto T., Kojima H., Imae N., Kong P., Ebihara M., and Prinz M. (1997b) Yamato-791093, a metal-sulfide-enriched H-group chondritic meteorite transitional to primitive IIE irons with silicate inclusions. *Antarct. Meteorite Res.* **10,** 335–353.

Jarosewich E. (1990) Chemical analyses of meteorites: A compilation of stony and iron meteorite analyses. *Meteoritics* **25,** 323–337.

Jones J. H. (1995) Experimental trace element partitioning. In *Rock Physics and Phase Relations, A Handbook of Physical Constants*, AGU Ref. Shelf **3,** 83, Amer. Geohys. Union.

Keil K., Stöffler D., Love S. G., and Scott E. R. D. (1997) Constraints on the role of impact heating and melting in asteroids. *Meteorit. Planet. Sci.* **32,** 349–363.

Koeberl C. (1986) Geochemistry of tektites and impact glasses. *Ann. Rev. Earth Planet. Sci.* **14,** 323–350.

Lindsley D. H. and Andersen D. J. (1983) A Two-pyroxene geothermometer. *Proc. 13th Lunar Planet. Sci. Conf. J. Geophys. Res. Suppl.* **18,** A887–A906.

Longhi J. (1991) Comparative liquidus equilibria of hypersthene-normative basalts at low pressure. *Amer. Mineral.* **76,** 785–800.

McKay G. A. (1986) Crystal/liquid partitioning of REE in basaltic systems: Extreme fractionation of REE in olivine. *Geochim. Cosmochim. Acta* **50,** 69–79.

McKay G., Wagstaff J., and Yang S.-R. (1986) Clinopyroxene REE distribution coefficients for shergottites: The REE content of the Shergotty melt. *Geochim. Cosmochim. Acta* **50,** 927–937.

Mayeda T. K. and R. N. Clayton (1980) Oxygen isotopic compositions of some unique meteorites. *Lunar Planet. Sci.* **XI,** 694–696 (abstract).

McBirney, A. R. (1993) *Igneous Petrology*, Second Edition, Jones and Bartlett Publishers, Inc., London, England, 508 pp.

McCoy T. J. (1995) Silicate-bearing IIE irons: Early mixing and differentiation in a core-mantle environment and shock-resetting of ages. *Meteoritics* **30,** 542–543 (abstract).

Olsen E. and Jarosewich E. (1970) The chemical composition of the silicate inclusions in the Weekeroo Station iron meteorite. *Earth Planet. Sci. Lett.* **8,** 261–266.

Olsen E. and Jarosewich E. (1971) Chondrules: First occurrence in an iron meteorite. *Science* **174,** 583–585.

Olsen E., Davis A., Clarke R. J., Jr., Schultz L., Weber H. W., Clayton R., Tayeda H., Jarosewich E., Sylvester P., Grossman L., Wang M.-S., Lipschutz M. E., Steele I. M. and Schwade J. (1994) Watson: A new link in the IIE iron chain. *Meteoritics* **29,** 200–213.

Papike J. J., Simon S. B., and Laul J. C. (1982) The lunar regolith: Chemistry, mineralogy, and petrology. *Rev. Geophys. Space Phys.* **20,** 761–826.

Papike J. J., Fowler G. W., and Shearer C. K. (1997) Evolution of the lunar crust: SIMS study of plagioclase from ferroan anorthosites. *Geochim. Cosmochim. Acta* **61,** 2343–2350.

Phinney W. C. and Morrison D. A. (1990) Partition coefficients for

calcic plagioclase: Implications for Archean anorthosites. *Geochim. Cosmochim. Acta* **54,** 1639–1654.

Prinz M., Nehru C. E., and Delaney J. S. (1982) Sombrerete; an iron with highly fractionated amphibole-bearing Na-P-rich silicate inclusions. *Lunar Planet. Sci.* **XIII,** 634–635 (abstract).

Prinz M., Nehru C. E., Delaney J. S., Weisberg M. and Olsen E. (1983) Globular silicate inclusions in IIE irons and Sombrerete: Highly fractionated minimum melts. *Lunar Planet. Sci.* **XIV,** 618–619 (abstract).

Rubin A. E., Jerde E. A., Zong P., Wasson J. T., Westcott J. W., Mayeda T. K. and Clayton R. N. (1986) Properties of the Guin ungrouped meteorite: The origin of Guin and of group-IIE irons. *Earth Planet. Sci. Lett.* **76,** 209–226.

Ruzicka A., Snyder G. A., and Taylor L. A. (1998) Mega-chondrules and large, igneous-textured clasts in Julesberg (L3) and other ordinary chondrites: Vapor-fractionation, shock-melting, and chondrule formation. *Geochim. Cosmochim. Acta* **62,** 1419–1442.

Schaal R. B. and Hörz. F. (1977) Shock metamorphism of lunar and terrestrial basalts. *Proc. 8th Lunar Sci. Conf.* 1697–1729.

Schaal R. B. Hörz F., Thompson T. D., and Bauer J. F. (1979) Shock metamorphism of granulated lunar basalts. *Proc. 10th Lunar Sci. Conf.* 2547–2571.

Schairer J. F. and Yoder H. S. (1961) Crystallization in the system Nepheline-Forsterite-Silica at one atmosphere pressure. *Carnegie Inst. Washington Yearbook* **60,** 141–144.

Scott E. R. D. and Wasson J. T. (1976) Chemical classification of iron meteorites—VIII. Groups IC, IIE, IIIF and 97 other irons. *Geochim. Cosmochim. Acta* **40,** 103–115.

Schwandt C. S. and McKay G. A. (1996) REE partition coefficients from synthetic diogenite-like enstatite and the implications of petrogenetic modeling. In *Workshop on evolution of igneous asteroids: Focus on Vesta and the HED meteorites*, LPI Tech. Report 96–02, pp. 25–26 (abstract).

Snyder G. A., Lee, D.-C., Ruzicka A., Prinz M., Taylor L. A. and Halliday A. N. (1999) Hf-W, Sm-Nd, and Rb-Sr isotopic studies of silicate inclusions in IIE irons: Evidence of late impact fractionation and mixing of silicate on iron meteorite parent bodies. In Press, *Earth Planet. Sci. Lett*.

Stöffler D., Bischoff A., Buchwald V., and Rubin A. E. (1988) Shock effects in meteorites. In *Meteorites and the Early Solar System* (ed. J. F. Kerridge and M. S. Matthews), pp. 165–202. Univ. Arizona Press.

Stöffler D., Keil K., and Scott E. R. D. (1991) Shock metamorphism of ordinary chondrites, *Geochim. Cosmochim. Acta* **55,** 3845–3867.

Takeda H., Hsu W., Huss G. R., and Wasserburg G. J. (1998) Silicate inclusions in the Colomera IIE iron and segregation of partial melts. *Lunar Planet. Sci.* **XXIX,** abstract #1677, Lunar and Planetary Institute, Houston (CD-ROM).

Taylor G. J., Keil K., McCoy T., Haack H., and Scott E. R. D. (1993) Asteroid differentiation: Pyroclastic volcanism to magma oceans. *Meteoritics* **28,** 34–52.

Walker R. J., and Papike J. J. (1981) The relationship of the lunar regolith <10 μm fraction and agglutinates. Part II: Chemical composition of agglutinate glass as a test of the "fusion of the finest fraction" (F^3) model. *Proc. Lunar Planet. Sc. Conf.* **12th,** 421–432.

Wasserburg G. J., Sanz H. G. and Bence A. E. (1968) Potassium-feldspar phenocrysts in the surface of Colomera, an iron meteorite. *Science* **161,** 684–687.

Wasson J. T. and Wang J. (1986) A non-magmatic origin of group-IIE iron meteorites. *Geochim. Cosmochim. Acta* **50,** 725–732.

Wosinski J. F., Beall G. H., and MacDowell J. F. (1967) Devitrification of tektite glass. *Science* **215,** 839–841.

Appendix 1. Literature and unpublished data for major-element abundances in silicate inclusions from IIE iron meteorites. All data in wt%, except Mg# (=Mg/[Mg + Fe^{2+}], atomic).

Inclusion	SiO_2	TiO_2	Al_2O_3	Cr_2O_3	FeO	MnO	MgO	CaO	Na_2O	K_2O	P_2O_5	Total	Mg#	ref.
Kod. F-1	69.6	0.05	15.1	0.23	0.54	0.03	1.77	2.25	7.8	2.25	0.4	100.02	0.85	[1]
Kod. F-2	66.7	0.18	10.9	0.97	2.01	0.10	6.0	5.5	5.7	1.58	0.49	100.13	0.84	[1]
Kod. 283-2	62.0	0.19	11.2	0.57	2.96	0.14	9.4	6.1	5.9	1.63	—	100.09	0.86	[1]
Kod. 283-1	57.7	0.35	6.0	1.1	3.9	0.23	13.7	12.6	3.4	0.81	0.34	100.13	0.90	[1]
Kod. 858-1	56.8	0.3	7.0	0.99	3.4	0.2	11.9	12.8	4.0	0.98	1.6	99.97	0.90	[1]
Kod. 858-2	66.8	0.01	18.4	0.01	0.17	0.01	0.53	1.06	9.5	2.76	0.74	99.99	0.84	[1]
Elga 1	63.7	0.10	10.3	0.53	2.0	0.1	5.9	8.1	3.5	3.8	2.01	100.04	0.57	[1]
Elga 2	66.5	0.11	10.7	0.56	2.06	0.11	6.0	6.5	3.5	3.9	—	99.94	0.56	[1]
Elga 3	65.0	0.21	9.8	0.66	2.36	0.12	6.9	8.1	3.2	3.5	0.11	99.96	0.56	[1]
Elga 4	72.3	0.01	15.2	0.01	0.29	0.01	0.66	0.42	5.0	5.8	0.4	100.10	0.55	[1]
Co. A-1	60.0	0.13	9.2	0.65	4.9	0.27	9.3	9.3	3.5	2.87	—	100.12	0.77	[1]
Co. A-2	64.2	0.04	16.1	0.20	1.52	0.09	3.1	3.3	6.1	5.3	—	99.95	0.78	[1]
Co. A-3	67.4	—	18.8	—	—	—	—	0.69	7.0	6.2	—	100.09	—	[1]
Co. A-4	62.1	0.13	15.8	1.8	2.41	0.10	2.96	3.7	5.9	5.1	0.11	100.11	0.69	[1]
Co. A-6	54.1	0.21	9.0	0.65	5.0	0.21	12.5	12.2	2.32	0.91	2.95	100.05	0.82	[1]
Co. A-7	66.2	0.01	18.9	—	0.23	0.02	0.44	0.80	7.1	6.2	0.08	99.98	0.77	[1]
Co. N-1†	56.8	0.22	4.2	0.72	7.51	0.45	14.1	10.7	1.76	1.25	1.03	98.74	0.77	[1]
Co. N-2‡	56.3	0.21	9.6	2.59	5.2	0.23	7.9	10.0	3.5	3.0	—	98.53	0.73	[1]
Co. N-3	59.2	0.12	10.1	1.03	4.3	0.20	7.8	10.2	3.9	3.2	—	100.05	0.76	[1]
Co. N-4	76.5	2.85	10.6	0.52	0.74	0.05	0.81	0.50	4.0	3.5	—	100.07	0.66	[1]
Co. N-5	56.9	0.18	12.4	2.43	3.7	0.15	5.1	8.5	4.7	3.9	2.04	100.00	0.71	[1]
Co. N-8	60.9	0.08	12.1	0.55	3.3	0.16	6.1	8.3	4.6	3.8	0.16	100.05	0.77	[1]
Co. N-14	63.1	0.69	7.8	0.80	4.2	0.20	7.7	10.1	3.0	2.42	—	100.01	0.77	[1]
Co. N-15	62.7	0.06	13	0.45	2.67	0.13	5.0	6.8	4.9	4.2	—	99.91	0.77	[1]
Co. N-20	64.6	0.57	16.8	0.13	1.83	0.14	3.3	0.79	6.3	5.5	—	99.96	0.76	[1]
Som. 1-2	58.4	0.67	14.4	0.09	3.9	0.14	4.5	7.8	5.6	0.15	4.3	99.95	0.67	[2]
Som. 1-3	52.0	1.06	12.6	0.11	4.9	0.17	5.5	11.6	4.6	0.12	7.3	99.96	0.67	[2]
Som. 1-4	58.8	1.8	13.6	0.13	5.2	0.17	5.4	6.0	5.6	0.15	3.1	99.95	0.65	[2]
Som. 1-5	57.7	0.38	14.3	0.10	4.1	0.16	5.1	8.3	5.3	0.14	4.5	100.08	0.69	[2]
Som. 1-7	54.2	0.69	13.2	0.11	4.6	0.17	5.4	10.4	4.9	0.13	6.2	100.00	0.68	[2]
Som. 1-11	59.3	0.36	17.2	0.06	2.69	0.10	3.1	8.0	5.8	0.15	3.4	100.16	0.67	[2]
Som. 1-15	59.2	0.36	16.9	0.07	3.1	0.12	3.7	7.7	5.6	0.15	3.2	100.10	0.68	[2]
Som. 1-18	59.0	0.41	14.0	0.32	4.0	0.15	4.7	7.4	5.7	0.15	4.2	100.03	0.31	[2]
Som. 2-7	59.0	0.41	14.0	0.32	4.0	0.15	4.7	7.4	5.7	0.15	4.2	100.03	0.68	[2]
Som S-2	54.6	0.69	12	2.84	7.0	0.26	7.0	6.6	4.8	0.13	4.1	100.02	0.64	[2]
Som. S-3	65.1	0.81	12.5	0.05	2.84	0.09	2.89	3.4	6.7	0.18	0.42	94.98	0.64	[2]
Som. S-4	55.8	0.64	14.9	1.16	4.3	0.16	4.5	8.6	5.2	0.14	4.5	99.90	0.65	[2]
Guin 1	65.6	0.77	13.3	0.29	2.7	0.10	4.9	5.9	6.6	0.47	0.10	100.73	0.76	[3]
Miles gab.	59.46	—	9.64	—	4.65	0.17	11.38	8.72	4.65	0.25	—	98.92	0.81	[4]
Miles cry.	63.86	1.58	15.1	0.01	0.63	0.01	1.21	3.82	9.13	0.88	3.78	100.01	0.77	[4]
Watson 1§	45.51	0.14	2.54	0.49	13.18	0.37	31.41	2.29	1.08	0.28	0.60	97.89	0.81	[5]
Net 1	48.4	0.31	2.73	0.89	13.1	0.52	29.4	2.44	1.13	0.28	0.80	100.00	0.80	[6]
WS OJ¶	54.54	0.29	5.22	2.76	10.67	0.59	16.24	5.16	1.8	0.2	0.1	97.62	0.81	[7]
WS 1A	72.5	0.39	15	0.01	0.97	0.04	0.78	2.7	6.3	0.69	0.64	100.02	0.59	[8]
WS 1B	60.7	0.63	9.3	0.59	6.3	0.56	9.8	7.6	3.9	0.41	0.34	100.13	0.73	[8]
WS 4	55.2	0.06	0.73	0.90	12.2	0.56	28.5	1.53	0.31	0.02	—	100.01	0.81	[8]
WS 5A	55.4	0.43	8.6	5.5	11.2	0.70	10.0	4.3	3.3	0.34	0.23	100.00	0.61	[8]
WS 5B	62.6	0.21	9.4	0.44	7.5	0.49	8.7	6.1	4.0	0.40	0.20	100.0	0.67	[8]
WS 6	61.9	0.24	8.2	0.61	7.8	0.53	9.5	7.6	3.4	0.35	0.10	100.23	0.68	[8]
WS 7	58.9	0.3	8.7	2.7	6.7	0.53	8.4	10.1	3.2	0.33	0.15	100.01	0.69	[8]

† Also 0.04 Ni, 0.23 S, 0.99 Fe. ‡ Also 0.05 Ni, 0.27 S, 1.16 Fe. § Also 0.13 Ni, 0.85 FeS, 0.24 Fe. ¶ Also 0.05 Ni, 0.12 H_2O^-, 0.98 C. [1] Unpublished data from Prinz et al. (1983); silicate inclusions in Kodaikanal (Kod.), Elga, Colomera (Co.); analyzed by modal reconstruction. [2] Unpublished data from Prinz et al. (1982); silicate inclusions in IIE-related iron Sombrerete (Som.); analyzed by modal reconstruction. [3] Large inclusions from the IIE-related iron Guin (Rubin et al., 1986); analyzed by modal reconstruction. [4] Representative gabbroic (gab.) and cryptocrystalline (cry.) inclusions in Miles (Ikeda and Prinz, 1996); analyzed by modal reconstruction. [5] Large inclusion in Watson (Olsen et al., 1994); analyzed by combination of wet-chemical and instrumental methods. [6] Portion of chondrule-bearing inclusion in Netschaëvo (Olsen and Jarosewich, 1971); analyzed by wet-chemical methods. [7] Average of 12 silicate inclusions in Weekeroo Station (Olsen and Jarosewich, 1970); analyzed by wet-chemical methods. [8] Unpublished data from Evensen et al. (1979); same inclusions as This Study; analyzed by modal reconstruction.